nature communications

Article

https://doi.org/10.1038/s41467-025-59522-7

A feedback loop at the *THERMOSENSITIVE PARTHENOCARPY 4* locus controls tomato fruit set under heat stress

Received: 16 July 2024

Accepted: 23 April 2025

Published online: 06 May 2025

Check for updates

Xiaonan Lu[1,6], Jianxin Wu[1,6], QianQian Shi[1], Shuai Sun[1], Yuan Cheng[2], Guozhi Zhou[2], Ren Li[1], Huanzhong Wang[3], Esther van der Knaap[4] & Xia Cui[1,5]

High temperatures compromise crop productivity worldwide, but breeding bottlenecks slow the delivery of climate-resilient crops. By investigating tomato fruit set under high temperatures, we discover a module comprising two linked genes, *THERMOSENSITIVE PARTHENOCARPY 4a* (*TSP4a*) and *TSP4b*, which encode the transcriptional regulators IAA9 and AINTEGUMENTA (ANT), respectively, to control thermosensitive parthenocarpy. *TSP4a* and *TSP4b* form a positive feedback loop upon heat stress to repress auxin signaling in ovaries. Natural *TSP4a* and *TSP4b* alleles bear regulatory-region polymorphisms and are differentially expressed to overcome the trade-off between fruit set and wider plant development. Gene editing of the *TSP4a* promoter and *TSP4b* 3′ UTR in open-chromatin regions results in expression down-regulation, increased parthenocarpy without yield penalties and maintenance of fruit-sugar levels without broad auxin-related pleiotropic defects in greenhouse-grown plants. These mechanistic insights into heat-induced parthenocarpy and auxin signaling in reproductive organs demonstrate breeding utility to safeguard tomato yield under warming scenarios.

Climate-change-associated extreme high temperature is a serious threat to global crop production, with every 1 °C increase in temperature, global production of major crops is predicted to decline by 3.1–7.4%[1]. Heat stress seriously damages pollen viability and female fertility, thereby heavily penalizing fruit set in tomato[2–4], the global market of which grew to $US17.865 billion in 2023[5]. In Florida, United States, which produces the most fresh tomatoes, heat stress causes decreases in production of 52–85%[6]. Therefore, fruit crops with a strong fruit-bearing ability are critical for maintaining consistent yields in variable environmental conditions.

Parthenocarpy is fruit production occurring without fertilization. It offers the possibility of improving fruit set when environmental conditions are adverse for pollen production and fertilization; moreover, the absence of seed is favored by consumers and can improve fruit quality in certain crops (e.g., banana, eggplant, persimmon, grape, and watermelon)[7]. Auxin is the first plant hormone known to induce parthenocarpy[8]. Exogenous application of auxin to unfertilized ovaries is widely used in commercial vegetable production to increase fruit set, but is laborious and often compromises fruit-quality characters[7]. Elevated auxin signaling induces parthenocarpy in fruit crops[7,9]. The

[1]State Key Laboratory of Vegetable Biobreeding, Sino–Dutch Joint Laboratory of Horticultural Genomics, Institute of Vegetables and Flowers, Chinese Academy of Agricultural Sciences, Beijing 100081, China. [2]State Key Laboratory for Managing Biotic and Chemical Threats to the Quality and Safety of Agro-Products, Institute of Vegetables, Zhejiang Academy of Agricultural Sciences, Hangzhou 310021, China. [3]Department of Plant Science and Landscape Architecture, University of Connecticut, Storrs, CT 06269, USA. [4]Department of Horticulture and Institute of Plant Breeding, Genetics & Genomics University of Georgia, Athens, GA 30602, USA. [5]Key Laboratory of Quality and Safety Control for Subtropical Fruit and Vegetable, Ministry of Agriculture and Rural Affairs, College of Horticulture Science, Zhejiang A&F University, Hangzhou 311300, China. [6]These authors contributed equally: Xiaonan Lu, Jianxin Wu. e-mail: cuixia@caas.cn

auxin response protein SlAUX/INDOLE-3-ACETIC-ACID 9 (SlIAA9) is a major repressor of fruit initiation, and its tomato null mutant, *entire*, shows strong parthenocarpy[10,11]. Loss of certain *AUXIN RESPONSE FACTOR* (*ARF*) transcription factors also enhances parthenocarpy in tomato[12–16]. Unfortunately, higher auxin activity invariably results in pleiotropic phenotypes, such as changes to plant and fruit morphology, which prevents widespread deployment in breeding programs[10,15,17,18].

A facultative parthenocarpic tomato line suitable for use in warm climates was developed in 1937[19]. Since then, only the *HOMEOBOX-LEUCINE ZIPPER PROTEIN 15 A* (*HB15A*) and *AGAMOUS-LIKE 6* (*AGL6*) alleles of historical *parthenocarpic* mutants *pat*/*pat-1* and *pat-K* respectively have been identified[20–22]. However, abnormal ovule development in these mutants results in few seeds that prohibit their exploitation in tomato breeding programs. It is therefore critical to identify other genetic resources that endow parthenocarpic fruit and viable seed, while also overcoming trade-offs between fruit set and plant development. Here, we discovered a locus comprising two genes, *THERMOSENSITIVE PARTHENOCARPY 4a* (*TSP4a*) and *TSP4b* that together form a positive feedback loop to regulate thermosensitive parthenocarpy in tomato. Natural *TSP4a* and *TSP4b* alleles function in auxin signaling by fine-tuning each other's expression levels to overcome the trade-off between fruit set and plant development, specifically under high temperature. Viable seeds produced at control temperatures and strong fruit-bearing ability without loss of desirable fruit sugars during heat stress in the greenhouse confirm their value for breeding climate-resilient crops to cope with changing weather patterns.

Results

TSP4 confers thermosensitive parthenocarpy

Heat stress often causes a dramatic reduction in fruit set in tomato because of pollen sensitivity and impaired fertilization[2–4]. To identify tomato accessions with sufficient fruit set at high temperature, we evaluated fruit set in 102 cultivated inbred tomato accessions collected from different countries under control-temperature conditions (daily mean temperature: 24 °C, peak temperature: 27 °C) and conditions simulating heat stress (daily mean temperature: 32 °C, peak temperature: 40 °C) near Beijing in 2021. Among them, accession XHS072 had robust fruit set under both conditions. By contrast, fruit set for Moneymaker (MM) was reduced by half under heat-stress conditions from that under control temperatures to about 22% (Fig. 1a, b). Approximately 70% of XHS072 fruits were seedless under heat stress, while seeded fruits were uniformly produced in Moneymaker, implying that most fruits produced by XHS072 were due to pollination-independent fruit set (Fig. 1c). Consistent with this, unpollinated XHS072 ovaries developed into normal-sized seedless fruits only under heat stress compared to unpollinated Moneymaker ovaries, further supporting that parthenocarpic fruits were induced by heat stress in XHS072 (Fig. 1d).

Toward identifying the locus underlying these phenotypes, we generated an F_2 population by crossing Moneymaker and XHS072 and evaluated parthenocarpy and seedless fruit set under heat stress. Bulked-segregant analysis coupled with whole-genome sequencing (BSA-seq) was performed using two pools with either low or high rates of seedless fruit[23]. A statistically significant locus on the long arm of chromosome 4 was identified that we named *THERMOSENSITIVE PARTHENOCARPY 4* (*TSP4*, Fig. 1e). We generated a pair of near-isogenic lines (NILs) to evaluate its contribution to fruit set under heat-stress conditions, named NIL-*TSP4*^{XHS072} and NIL-*TSP4*^{MM} that differ by approximately 860 kb at this locus. More seedless fruits were produced by NIL-*TSP4*^{XHS072} plants than the NIL-*TSP4*^{MM} only under heat stress (Fig. 1f). This result supports the hypothesis that *TSP4* confers thermosensitive parthenocarpy in tomato.

To explore the reason behind the relatively large proportion of unfertilized NIL-*TSP4*^{XHS072} fruits and precocious fruit set prior to anthesis under heat stress, we examined ovary development. Unpollinated ovaries had expanded at −2 days post anthesis (DPA) under heat stress (Supplementary Fig. 1a, b). Such precocious ovary enlargement positioned the stigma out of reach of the stamen, thereby reducing self-pollination and contributing to the development of seedless fruit (Supplementary Fig. 1c). The enlarged NIL-*TSP4*^{XHS072} ovaries were reminiscent of floral auxin application, which is involved in parthenocarpic fruit set[9,24]. We therefore quantified indole-3-acetic acid contents in −2 DPA NIL-*TSP4*^{MM} and NIL-*TSP4*^{XHS072} by HPLC–MS/MS and saw elevation in ovaries isolated from plants grown under heat stress for both NILs, whereas no obvious differences were found at the control temperature (Supplementary Fig. 1d). These results implied that the elevated auxin contents observed in ovaries upon heat stress are not affected by *TSP4*.

TSP4a and *TSP4b* respectively encode SlIAA9 and SlANT transcriptional regulators

To clone the *TSP4* gene, we conducted a high-resolution linkage analysis with 4,416 individuals of heterozygous NILs. Unexpectedly, recombinants with the same genotype displayed different parthenocarpic phenotypes. We analyzed the phenotypes of different recombinants and considered that two genes, designated *TSP4a* and *TSP4b*, instead of one, were potentially located at this locus. By comparing parthenocarpy between the offspring of NIL-*TSP4a*$^{MM/XHS072}$ *TSP4b*^{XHS072}, we delimited the *TSP4a* locus to a 30-kb region, comprising only one gene *Solyc04g076850* encoding SlIAA9 (Fig. 1g and Supplementary Fig. 2a). According to differential parthenocarpy of NIL-*TSP4a*^{XHS072} *TSP4b*$^{MM/XHS072}$ offspring, *TSP4b* was mapped to a 54-kb region, in which *Solyc04g077470*, *Solyc04g077480* and the 3′ UTR of *Solyc04g077490* were located (Fig. 1g). Among them, only *Solyc04g077490*, encoding a putative ortholog of *SlAINTEGUMENTA* (*SlANT*, Supplementary Fig. 2b), was differentially expressed in the −2 DPA ovaries of NILs-*TSP4* under high temperature (Fig. 1g, Supplementary Fig. 3), implying that this gene was the most likely the candidate for *TSP4b*.

Toward confirming whether *SlIAA9* and *SlANT* correspond to *TSP4a* and *TSP4b*, we carried out in situ hybridization to determine the expression patterns on transverse sections. Histological analysis of hybridization signals in reproductive tissues showed that *TSP4a* transcript had significant accumulation throughout the ovary, whereas *TSP4b* was mainly accumulated in the ovule and placenta. These results implied functionality for these two genes during fruit set (Supplementary Fig. 4).

We next compared Moneymaker and XHS072 genome sequences and found a single-nucleotide polymorphism (SNP) in the *SlIAA9* coding region, which causes an amino-acid substitution from isoleucine to serine at position 94 (I94S, Supplementary Fig. 5a). However, this substitution is potentially inconsequential for protein function because it is a conservative substitution. In addition, 4 2 SNPs and 7 indels in the *SlIAA9* promoter, and 12 SNPs and 4 indels in the *SlANT* 3′ UTR were found (Supplementary Fig. 5b). *SlIAA9* and *SlANT* expression levels were statistically significantly reduced in NIL-*TSP4*^{XHS072} compared to NIL-*TSP4*^{MM} from −2 DPA to 6 DPA under heat stress, but not at control temperatures (Fig. 1h, Supplementary Fig. 6a), suggesting that *SlIAA9* and *SlANT* are the candidate genes for *TSP4a* and *TSP4b*. Similar expression patterns in leaves also confirmed that regulatory changes in the promoter and 3′ UTR respectively account for the variation in their expression levels (Supplementary Fig. 6b).

To verify the functions of *TSP4a* and *TSP4b*, we generated knockout mutants in the non-parthenocarpic parent Moneymaker by CRISPR–Cas9 (Supplementary Fig. 7a, b). The recovered *tsp4acr* mutants produced 51% seedless fruits under control temperatures (Fig. 1i) similar to other tomato *SlIAA9* mutants and knock-down lines[10,25]. When the *tsp4acr* plants were grown under heat-stress conditions, seedless fruit increased to 87%. *tsp4bcr* plants instead produced 16% seedless fruits under control temperatures and 32%

seedless fruits under heat stress. When *TSP4b* was knocked out in the parthenocarpic XHS072 background, unpollinated ovaries could develop into seedless fruits at control temperatures (Supplementary Fig. 7c, d). The *tsp4bcr3* and *tsp4bcr4* mutants bore 70% seedless fruits at control temperatures and completely (i.e. 100%) seedless fruits upon heat stress, greater than XHS072 (Supplementary Fig. 7e). Additionally, *tsp4a/4bcr* double mutants in the Moneymaker background displayed even stronger parthenocarpy (~100%) under both control and heat-stress conditions (Fig. 1i). These data revealed that XHS072 is a weak allele, in which the functions of *TSP4a* and *TSP4b* are not completely lost, and *TSP4a* and *TSP4b* play major roles in the regulation of tomato parthenocarpy.

Natural *TSP4a* and *TSP4b* alleles improve tomato yield at high temperatures

To examine whether allelic variation in *TSP4a* and *TSP4b* affects tomato yield at high temperature, we generated a series of alleles by genetic crossing with different combinations of *TSP4a* and *TSP4b* haplotypes. Remarkably, only the combinations of $TSP4a^{XHS072}/4b^{MM/XHS072}$, $TSP4a^{MM/XHS072}/4b^{XHS072}$ and $TSP4a^{XHS072}/4b^{XHS072}$ lines

Fig. 1 | The *TSP4* locus regulates thermosensitive parthenocarpy in tomato. **a** Shoot and fruit phenotypes for 120-d old wild-type Moneymaker and XHS072 plants under high-temperature conditions in the greenhouse. Scale bar = 10 cm. Fruit-set rate (**b**) and seedless-fruit rate (**c**) for Moneymaker and XHS072 under control and heat-stress conditions in the greenhouse, $n = 5$ plants. **d** Sepal and fruit phenotypes of 120-d old Unpollinated and Pollinated Moneymaker and XHS072 plants under control and heat-stress conditions in the greenhouse. Scale bar = 1 cm. **e** SNP ratios on chromosome 4 based on QTL-Seq and bulk-segregant analysis. The highest peak indicates the *TSP4* locus. **f** Percentage of seedless fruit in NIL-$TSP4^{MM}$ ($n = 10$ and 9 plants) and NIL-$TSP4^{XHS072}$ ($n = 5$ and 7 plants) under control and heat-stress conditions in the greenhouse. **g** Fine mapping of *qTSP4* on chromosome 4. Solid lines indicate genotyping markers (M1–10) and numbers of recombinant plants. 'Pat' and 'No pat' represent the parthenocarpy and non-parthenocarpy phenotypes, respectively. Orange and purple indicate chromosomal regions homozygous with Moneymaker and XHS072, respectively. **h** *TSP4a* and *TSP4b* expression in −2 DPA ovaries isolated from NIL-$TSP4^{MM}$ and NIL-$TSP4^{XHS072}$ plants grown under control and heat-stress conditions. Data are the mean ± S.D. of n = 3 biologically independent replicates and relative expression was normalized to *UBIQ3*. Data were compared by two-tailed Student's *t*-test, $^{**}P < 0.01$, n.s. non-significant ($P > 0.05$). **i** Percentage of seedless fruit for wild-type Moneymaker, *tsp4acr* single mutants, *tsp4bcr* single mutants and *tsp4a/4bcr* double-mutant plants grown under control and heat-stress conditions, $n = 5$ plants. Box edges in (**b**, **c**, **f**, **i**) represent the 0.25 and 0.75 quantiles, the center line indicate median values, and the bar shows the range from minimum to maximum values. Data in (**b**, **c**, **f**, **i**) are the mean ± S.D. and were compared by two-tailed Mann–Whitney–U test, $^{*}P < 0.05$, $^{**}P < 0.01$, n.s. non-significant ($P > 0.05$). Source data are provided as a Source Data file.

produced seedless fruits under heat stress compared to the $TSP4a^{MM}/4b^{MM}$ lines (Fig. 2a). Consistent with this finding, fruit numbers for these haplotypes were increased by 44%, 26% and 81% respectively, under heat stress (Fig. 2b) without appreciably affecting fruit fresh weight (Fig. 2c). Other plant and leaf morphological characteristics were largely comparable compared to the $TSP4a^{MM}/4b^{MM}$ lines, although alleles carrying $TSP4b^{XHS072}$ flowered earlier (Fig. 2d and Supplementary Fig. 8a). The increase in fruit set and unchanged fruit mass dramatically improved tomato yields, with a 67% and 76% yield increase observed for $TSP4a^{XHS072}/4b^{XHS072}$ under heat stress when grown in Beijing, Nankou in 2023 and Shunyi (both near Beijing) in 2022, respectively (Fig. 2e and Supplementary Fig. 8b). Notably, there was no penalty on fruit sugar contents (an important sensory trait for consumers), with higher fructose and glucose contents seen in red ripe fruits of $TSP4a^{XHS072}$ lines (Supplementary Fig. 8c). These results demonstrated that natural alleles of *TSP4a* and *TSP4b* increase tomato yield without major negative effects under heat stress.

Different from natural *TSP4a* and *TSP4b* alleles, *tsp4acr* mutants revert from compound to simple leaves (Fig. 2f and Supplementary Fig. 8d), mimicking *entire* mutants with a shorter stature[10,11]. Compared with Moneymaker controls, *tsp4acr* and *tsp4bcr* mutants produced smaller fruits and fruit weights were reduced to 35% and 30%, respectively (Fig. 2f, g). Unlike *ANT* which regulates shoot, flower and ovule development in Arabidopsis[26,27], the tomato *tsp4bcr* mutants in the Moneymaker and XHS072 backgrounds only exhibit shorter stature (Supplementary Fig. 8d–f). Notably, shorter stature, simple leaves, and smaller and abnormal fruits were observed in the *tsp4a/4bcr* double mutants (Fig. 2f, g and Supplementary Fig. 8d, g), indicating the genetic interaction between *TSP4a* and *TSP4b* in facilitating fruit enlargement and leaf development. Similar to $TSP4b^{XHS072}$ alleles, only the *tsp4bcr* single mutants and *tsp4a/4bcr* double mutants displayed early flowering, suggesting that only *TSP4b* contributes to repressing the floral transition (Supplementary Fig. 8h, i). Although the *tsp4acr* and *tsp4a/4bcr* mutants produced approximately twice as many fruits as Moneymaker controls under heat stress, non-significant yield increases were observed for *tsp4acr* mutants and *tsp4a/4bcr* double mutant under heat stress in the greenhouse (Fig. 2h, i and Supplementary Fig. 8j). These results suggested knock-out mutations in *TSP4a* and *TSP4b* led to a reduction in fruit weight and pleiotropic phenotypes that limit yield improvement.

TSP4a and *TSP4b* comprise a positive feedback regulatory loop to regulate their expression

Certain *TSP4a* and *TSP4b* haplotype combinations bear almost no seedless fruits under heat stress (see Results section for Fig. 2a). To further explore the molecular basis of this phenotype, we compared *TSP4a* and *TSP4b* expression levels among different haplotype combinations under heat stress. Although *TSP4a* and *TSP4b* expression was markedly reduced in −2 DPA ovaries isolated from $TSP4a^{XHS072}/4b^{MM}$ and $TSP4a^{MM}/4b^{XHS072}$ plants compared to $TSP4a^{MM}/4b^{MM}$, the lowest expression levels were detected in $TSP4a^{XHS072}/4b^{XHS072}$ ovaries (Fig. 3a), implying that down-regulation of *TSP4a* and *TSP4b* is associated with the parthenocarpic phenotype. Similar down-regulation was seen in the gene-edited mutants. These data imply that the expression of *TSP4a* and *TSP4b* functions in a positive regulatory loop (Fig. 3b).

Since high temperature enhances parthenocarpic fruit set for NIL-$TSP4^{XHS072}$ plants, we explored whether *TSP4a* and *TSP4b* expression is responsive to heat stress. Upon exposure of Moneymaker plants to 35 °C for 8 h, both genes were rapidly induced (Fig. 3c). However, the heat-stress-induced transcription of *TSP4a* in the *tsp4bcr* mutants and *TSP4b* in the *tsp4acr* mutants was dramatically compromised (Fig. 3d), implying that both *TSP4a* and *TSP4b* are required for their induction upon heat stress. *TSP4a* and *TSP4b* expression was also induced within 1 h of auxin supplementation (Fig. 3e), similar to other *AUX/IAA* genes[28]. This induction was also compromised in the *tsp4bcr* and *tsp4acr* mutants, respectively (Fig. 3f), indicating that *TSP4a* and *TSP4b* are both necessary for auxin-dependent induction. Taken together, these data support a model whereby *TSP4a* and *TSP4b* are required for increasing the expression of each other in response to auxin and heat stress.

SlARF2a–TSP4a and TSP4b directly activate the transcription of *TSP4b* and *TSP4a*

To explore how TSP4a and TSP4b regulate each other's expression, we first analyzed *TSP4a* promoter and *TSP4b* 3′ UTR sequences. Based on the conserved motif [gCAC(A/G)N(A/T)TcCC(a/g)ANG(c/t)] bound by the transcription factor ANT[29], several binding sites on the *TSP4a* promoter were identified. Chromatin immunoprecipitation followed by quantitative polymerase chain reaction (ChIP–qPCR) was used to test whether TSP4b directly binds to these sequences in $35S_{pro}$:*TSP4b–YFP–HA* transgenic plants, which could partially rescue parthenocarpic phenotypes of NIL-$TSP4^{XHS072}$ (Supplementary Fig. 9). Enrichment of TSP4b–YFP–HA on the P2 and P3 regions indicates that TSP4b binds to the *TSP4a* promoter (Fig. 4a). Dual luciferase reporter assays revealed that TSP4b–FLAG activates *TSP4a* transcription (Fig. 4b). All these results indicate that TSP4b bind to the *TSP4a* promoter to activate its expression.

SlIAA9 is an AUX/IAA protein that participates in regulating the auxin signaling pathway through its physical interaction with AUXIN RESPONSE FACTORS (ARFs). When SlIAA9 interacts with ARFs, it inhibits the transcriptional regulatory function of ARFs[30]. We first analyzed sequence variation of the *TSP4b* 3′ UTR between XHS072 and MM and found that only the binding sites for ARF2 constitute sequence differences. We therefore investigated the physical interaction between TSP4a and SlARF2a or SlARF2b. Yeast two-hybrid assay showed that SlARF2a could interact with TSP4a through its PB1 (Phox and Bem1) domain (Fig. 4c and Supplementary Fig. 10a, b). Bimolecular fluorescence complementation (BiFC) assays revealed this interaction occurs in the nucleus (Fig. 4d and Supplementary Fig. 10c). Overexpression of $SlARF2a^{Tr}$–*YFP–HA* (a truncated variant of ARF2a lacking

https://doi.org/10.1038/s41467-025-59522-7

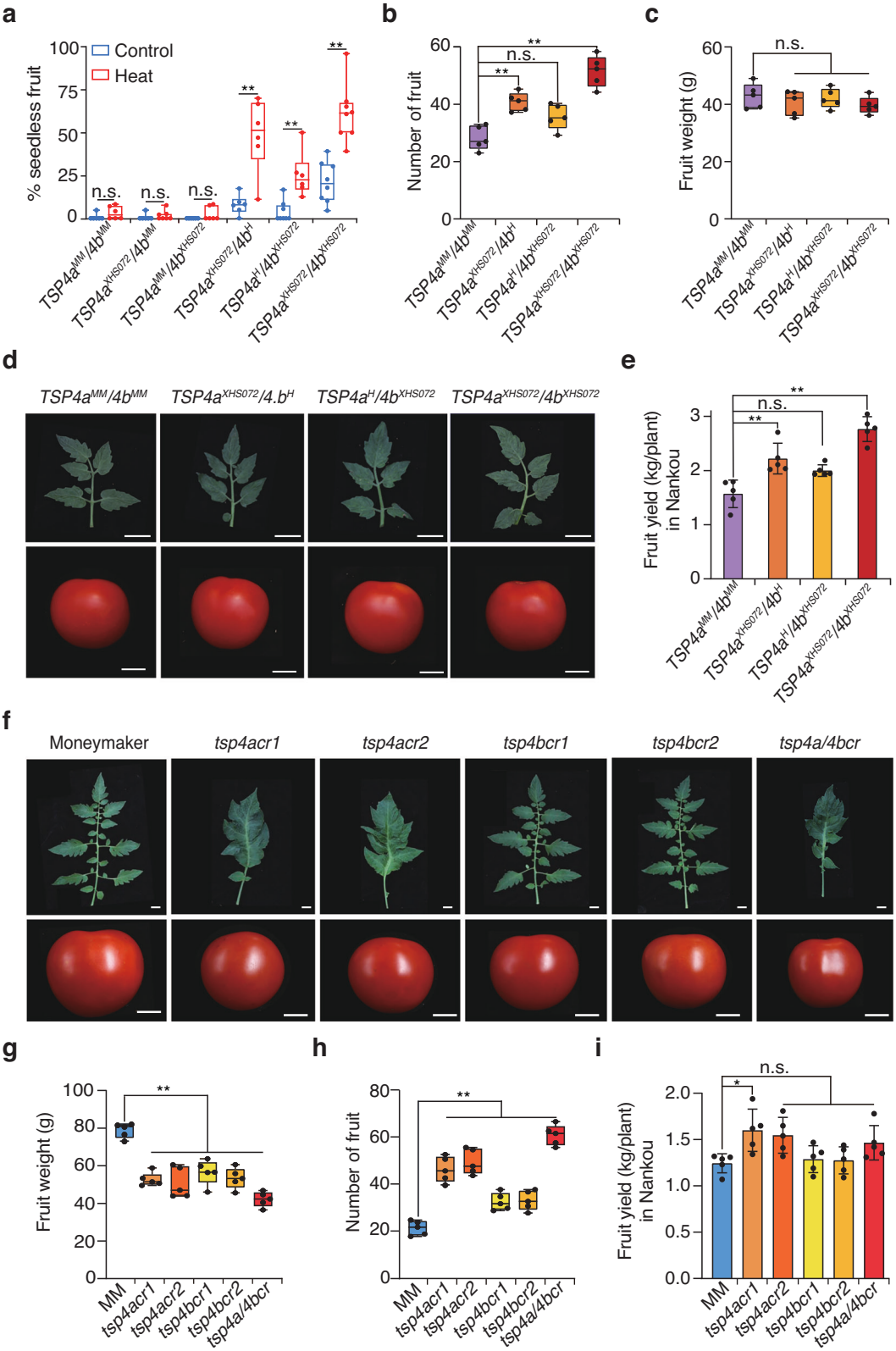

the PB1 domain) in the MM background demonstrated that SlARF2aOE^{Tr}-L1 and SlARF2a^{Tr}OE-L2 lines exhibited parthenocarpic phenotype, similar to that observed in *tsp4bcr* mutants. This result suggests that SlARF2a participates in regulating parthenocarpy (Fig. 4e).

To determine whether SlARF2a could bind to the *TSP4b* 3′ UTR, we performed ChIP–qPCR using SlARF2a^{Tr}OE-L1 plants. A statistically significant enrichment of SlARF2a^{Tr}–YFP–HA was observed at P3, P4 and P6 regions, but not at other assayed ARF2a-recognized sites, indicating that SlARF2a could bind to the *TSP4b* 3′ UTR (Fig. 4f). We also found that *TSP4b* expression was dramatically reduced in SlARF2a^{Tr}OE plants (Fig. 4g). Moreover, when SlARF2a–FLAG was co-expressed with $35S_{pro}$:*LUC*:*TSP4b*$_{UTR}$ in *N. benthamiana* leaves, chemiluminescence intensity was obviously reduced compared with

Fig. 2 | Natural *TSP4a* and *TSP4b* alleles enhance yield under heat stress. **a** Percentage of seedless fruit for natural alleles with different combinations, including $TSP4a^{MM}4b^{MM}$ ($n = 6$ plants), $TSP4a^{XHS072}4b^{MM}$ ($n = 6$ and 7 plants), $TSP4a^{MM}4b^{XHS072}$ ($n = 6$ plants), $TSP4a^{XHS072}4b^{H}$(n = 6 plants), $TSP4a^{H}4b^{XHS072}$ ($n = 8$ and 6 plants), $TSP4a^{XHS072}4b^{XHS072}$ (n = 8 plants) grown under control and heat-stress conditions in the greenhouse. 'H' represents the heterozygous haplotype of Moneymaker/XHS072. Data are the mean ± S.D. and were compared by two-tailed Mann−Whitney−U test, $^{**}P < 0.01$, n.s. non-significant ($P > 0.05$). Number of fruit (**b**) and fruit weight (**c**) for alleles with different combinations of *TSP4a* and *TSP4b* haplotypes from plants grown under heat-stress conditions in the greenhouse. **d** Leaf and fruit phenotypes of alleles with different combinations of *TSP4a* and *TSP4b* haplotypes from 120-d old plants grown under heat-stress conditions in the greenhouse. Scale bar = 2 cm. **e** Fruit yield from $TSP4a^{MM}4b^{MM}$, $TSP4a^{XHS072}4b^{H}$, $TSP4a^{H}4b^{XHS072}$ and $TSP4a^{XHS072}4b^{XHS072}$ plants grown under heat-stress conditions in the greenhouse in Beijing, Nankou, 2023. **f** Leaf and fruit phenotypes of Moneymaker, *tsp4acr* single mutants, *tsp4bcr* single mutants and *tsp4a/4bcr* double mutants from 120-d old plants grown under heat stress in the greenhouse. Scale bars, 2 cm. Fruit weight (**g**), fruit number (**h**) and fruit yield (**i**) for Moneymaker, *tsp4acr* single mutants, *tsp4bcr* single mutants and *tsp4a/4bcr* double mutants grown under heat-stress conditions in the greenhouse in Beijing, Nankou, 2023. Box edges in (**a**–**c**, **g, h**) represent the 0.25 and 0.75 quantiles, the center line indicate median values, and the bar shows the range from minimum to maximum values. Data in (**b**, **c**, **e**, **g**–**i**) are the mean ± S.D. of $n = 5$ plants. The effect of genotype on y-axis traits was determined by one-way ANOVA with multiple comparisons and Tukey post-hoc test ($\alpha = 0.05$). $^{*}P < 0.05$, $^{**}P < 0.01$, n.s. non-significant ($P > 0.05$). Source data are provided as a Source Data file.

the empty vector control, indicating that SlARF2a repress *TSP4b* transcription. Fluorescence intensity was restored by adding *TSP4a-FLAG* in the SlARF2a-FLAG/$35S_{pro}$:*LUC:TSP4b*$_{UTR}$ co-expression system, whereas co-expression with the truncated *SlARF2a*^{Tr}-*FLAG*/$35S_{pro}$:*LUC:TSP4b*$_{UTR}$ failed to rescue this fluorescence signal (Fig. 4h). These results suggest that TSP4a interacts with SlARF2a, hindering SlARF2a from repressing *TSP4b* transcription through binding its 3' UTR.

TSP4a and *TSP4b* directly regulate downstream auxin-responsive genes

To explore how TSP4a and TSP4b regulate heat stress and auxin responses during fruit initiation, we compared transcriptomes of NIL-*TSP4*^{MM} and NIL- *TSP4*^{XHS072} -2 DPA ovaries from plants grown under control and heat-stress conditions (Supplementary Fig. 11a). In NIL-*TSP4*^{MM} and NIL-*TSP4*^{XHS072} ovaries, 341 genes were up-regulated and 322 were down-regulated under heat stress (Supplementary Fig. 11b and Supplementary Data 1). The 'temperature stimulus' gene-ontology (GO) term was enriched in the up-regulated genes, including several *HEAT-SHOCK PROTEIN* (*HSP*) genes (Supplementary Fig. 11c, d). A total of 516 genes and 468 genes were up- or down-regulated respectively in the NIL-*TSP4*^{XHS072} ovaries under heat stress (Supplementary Fig. 11e and Supplementary Data 2), with 'auxin response' and 'floral-organ development' in up-regulated genes. 'Jasmonic-acid signaling' and 'plant organ identity' were enriched in the down-regulated genes (Supplementary Fig. 11f). These included the established warm-temperature-induced auxin-signaling genes such as *SAUR*, *AUX/IAA* and *ARF* (Supplementary Fig. 11g). These results indicated that the expression of these temperature-induced auxin-responsive genes depended on both *TSP4a* and *TSP4b*.

Among genes in the auxin-response pathway, two early-fruit-development-related genes, *EXPANSIN 5* (*EXP5*, encoding a cell-wall protein involved in cell-wall modifications) and *ACC OXIDASE 4* (*ACO4*, encoding an enzyme involved in ethylene biosynthesis) were specifically activated or repressed in NIL-*TSP4*^{XHS072} under heat stress (Fig. 5a and Supplementary Fig. 11h)[13]. *EXP5* expression was higher and *ACO4* expression was lower in the *tsp4acr* and *tsp4bcr* single mutants, and further up-regulated in the *tsp4a/4bcr* double mutants under heat stress compared to wild-type plants (Fig. 5a). These results implied that *TSP4a* and *TSP4b* together control *EXP5* and *ACO4* expression.

Consistent with their regulatory roles in auxin signaling, TSP4a and TSP4b were localized in the nucleus (Supplementary Fig. 12). However, TSP4a physically interacts with ARF7 to regulate *EXP5* and *ACO4* expression by ARF7 directly binding to their promoters[13]. To explore whether TSP4b−YFP−HA regulates *EXP5* and *ACO4* transcription by direct binding, we performed ChIP−qPCR. The results showed that TSP4b−YFP−HA binds to the P3 region of the *EXP5* promoter, and the P2 and P4 regions of the *ACO4* promoter (Fig. 5b). Transiently co-expression of TSP4b−FLAG with the $EXP5_{pro}$:*LUC and* $ACO4_{pro}$:*LUC* in *N. benthamiana* leaves revealed that TSP4b-FLAG activates *EXP5* and represses *ACO4* expression respectively (Supplementary Fig. 13).

Consistent with the model that the *TSP4a*−*TSP4b* feedback loop directly controls *EXP5* and *ACO4* expression, *EXP5* induction and *ACO4* repression after heat stress and auxin treatment were statistically significantly enhanced in the *tsp4acr* and *tsp4bcr* mutants compared to Moneymaker and untreated control plants (Fig. 5c, d). These results indicated that *TSP4a* and *TSP4b* participate in auxin signaling by directly regulating downstream genes under heat stress.

TSP4a and TSP4b influence auxin signaling

SlIAA9 is a negative regulator of auxin signaling and this pathway is elevated in *entire* mutants[10]. We compared *EXP5* and *ACO4* expression in NIL-*TSP4*^{MM} and NIL-*TSP4*^{XHS072} plants, together with *tsp4acr*, *tsp4bcr* and *tsp4a/tsp4bcr* mutants and wild-type Moneymaker controls. *EXP5* up-regulation and *ACO4* down-regulation were greater in *tsp4acr* mutant ovaries than those of NIL-*TSP4*^{XHS072} when compared to the corresponding controls. Much higher *EXP5* expression and extremely low *ACO4* expression still was detected in *tsp4a/tsp4bcr* double-mutant ovaries (see Results section for Fig. 5a).

To test whether different levels of *TSP4a* and *TSP4b* expression influence auxin responsiveness, we compared root formation and hypocotyl-segment elongation in plants grown at 25 °C and 35 °C. In *tsp4acr* mutants, the auxin analog α-naphthalene acetic acid (NAA) promoted root formation at concentrations above 10 nM both at 25 °C and 35 °C, whereas NAA promoted root formation from NIL-*TSP4*^{XHS072} cotyledon explants above concentrations of 10 nM only at 35 °C. At 25 °C, roots were formed from NIL-*TSP4*^{XHS072} at 20 nM, suggesting these plants are more sensitive to auxin under heat stress. Compared with NIL-*TSP4*^{XHS072} cotyledon explants, *tsp4acr* induced more roots were induced at the same concentration, indicating that *tsp4acr* mutants are more sensitive than NIL-*TSP4*^{XHS072} plants to auxin (Fig. 5e and Supplementary Fig. 14). Hypocotyl-elongation trends for *tsp4acr* and NIL-*TSP4*^{XHS072} plants grown at 25 °C and 35 °C in a concentration series support an interpretation that *tsp4acr* plants are more sensitive to auxin (Fig. 5f), albeit the NAA concentrations used exceed physiological ranges. Taken together, *TSP4a-SlARF2a* and *TSP4b* act in a positive regulatory loop to repress auxin signaling during fruit set and plant development under heat stress (Fig. 5g).

Targeted manipulation of *TSP4a* and *TSP4b* dosage conditionally improves yield under heat stress in the greenhouse

Down-regulation of *TSP4a* and *TSP4b* expression in NIL-*TSP4*^{XHS072} at high temperatures results in parthenocarpy (see Results section for Fig. 3a). This characteristic of the XHS072 haplotype enhances tomato adaptability and improves fruit productivity under heat stress, without obvious negative phenotypes. These features are of substantial interest to commercial tomato production and represent an important appearance trait for consumers of fresh table tomatoes. To estimate the potential breeding value of the *TSP4*^{XHS072} haplotype, we crossed XHS072 with XHS369, which is a tomato accession with the *TSP4*^{MM} haplotype with low fruit set at high temperature (Fig. 6a), but has good

https://doi.org/10.1038/s41467-025-59522-7

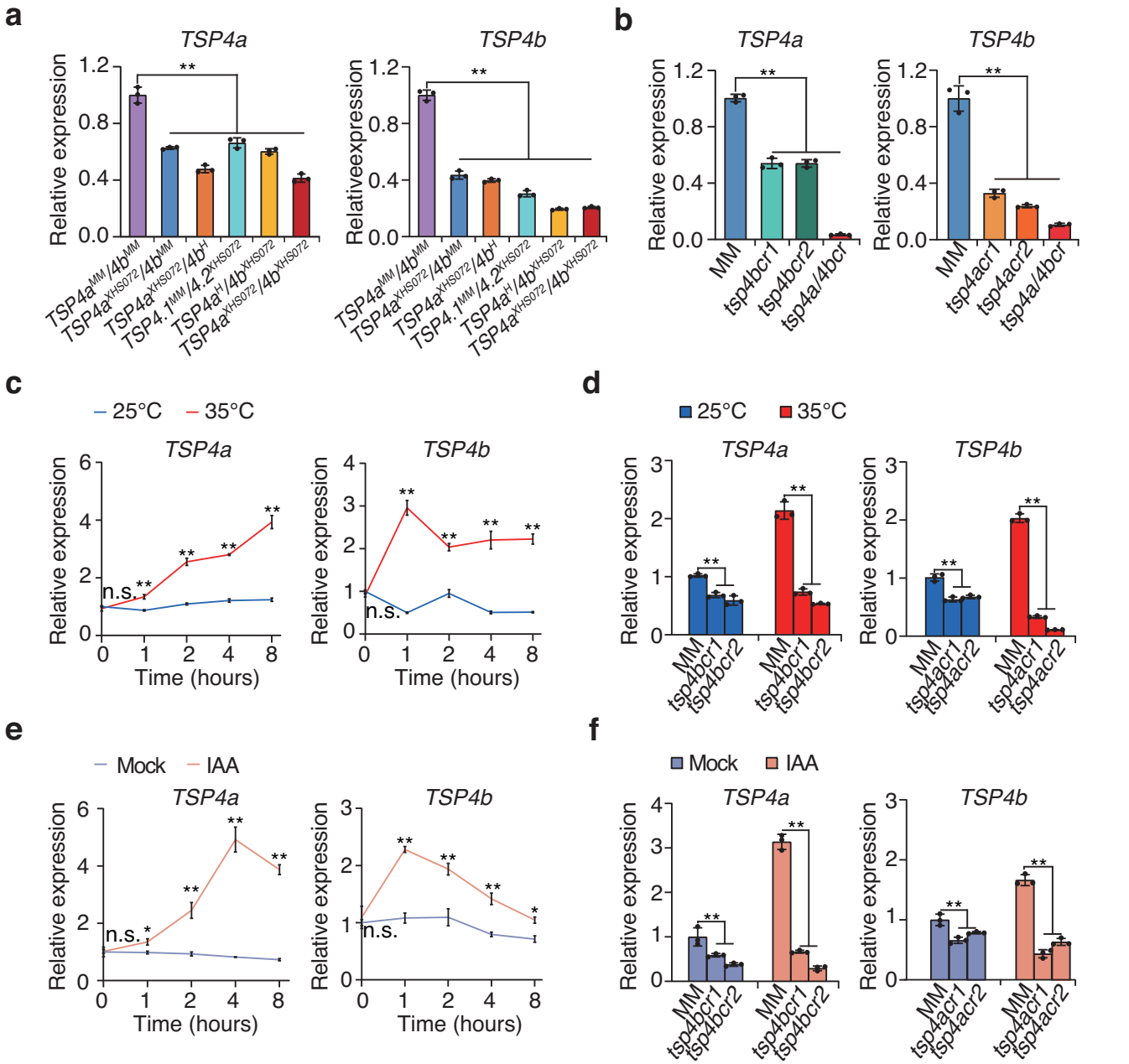

Fig. 3 | *TSP4a* and *TSP4b* comprise a positive feedback loop activated in response to heat stress and auxin cues. a *TSP4a* and *TSP4b* expression in −2 DPA ovaries isolated from plants carrying alleles with different combinations of *TSP4a* and *TSP4b* haplotypes grown under high temperature. **b** *TSP4a* and *TSP4b* expression in −2 DPA ovaries isolated from Moneymaker, *tsp4bcr* single mutants, *tsp4acr* single mutants and *tsp4a/4bcr* double mutants grown under high temperature. **c** Time course of *TSP4a* and *TSP4b* expression at 25 °C and 35 °C. Seedlings were grown to the 4-leaf stage at 25 °C under 12-h light/12-h darkness and then transferred into 25 °C temperature and constant illumination for 5 d. Afterward, seedlings were transferred to 35 °C and constant illumination. Leaf samples were collected at the indicated time points for analysis. **d** *TSP4a* and *TSP4b* expression in Moneymaker, *tsp4acr* and *tsp4bcr* single mutants after exposure to 25 °C and 35 °C for 2 h. **e** Time course of *TSP4a* and *TSP4b* expression after mock and 10 μM IAA treatment. Twelve-day-old seedlings were incubated on 1/2 MS medium under 25 °C and 12-h light/12-h dark in a growth chamber. Seedlings were transferred to liquid 1/2 MS medium with or without 10 μM IAA. Samples were collected and analyzed at the indicated time points. **f** *TSP4a* and *TSP4b* expression in Moneymaker and *tsp4bcr* single mutants or *tsp4acr* single mutants treated with 10 μM IAA for 2 h. Data in (**a**–**f**) are the mean ± S.D. of $n = 3$ biologically independent replicates and relative expression was normalized to *UBIQ3*. Data in (**a**–**c**, **e**) were determined by one-way ANOVA with multiple comparisons and Tukey post-hoc test ($\alpha = 0.05$). $^{**}P < 0.01$. Data in (**d**, **f**) were determined by two-way ANOVA with multiple comparisons and Tukey post-hoc test ($\alpha = 0.05$). $^{**}P < 0.01$. Source data are provided as a Source Data file.

taste, uniform fruit appearance and bright color. After backcrossing for four generations followed by marker-assisted selection, NIL-*XHS369*^{XHS072} plants displayed a high ratio of seedless fruits without other noticeable phenotypic changes under heat stress in the greenhouse (Fig. 6b and Supplementary Fig. 15a, b). Compared with XHS369, the similar fruit weight enhanced yield by approximately 77% in NIL-*XHS369* ^{XHS072} under heat-stress conditions (Fig. 6c–e).

Because down-regulation of *TSP4a* and *TSP4b* leads to parthenocarpy in XHS072 under heat stress, we wondered whether targeted edits to their regulatory regions, such as the promoter or UTRs, could produce a series of alleles with high parthenocarpic fruit set without undesirable phenotypes by altering expression levels. We generated gene-edited lines in the Moneymaker background with deletions in the *TSP4a* promoter ("*pro*") and *TSP4b* 3′ UTR ("*utr*") around ATAC-seq peaks

https://doi.org/10.1038/s41467-025-59522-7

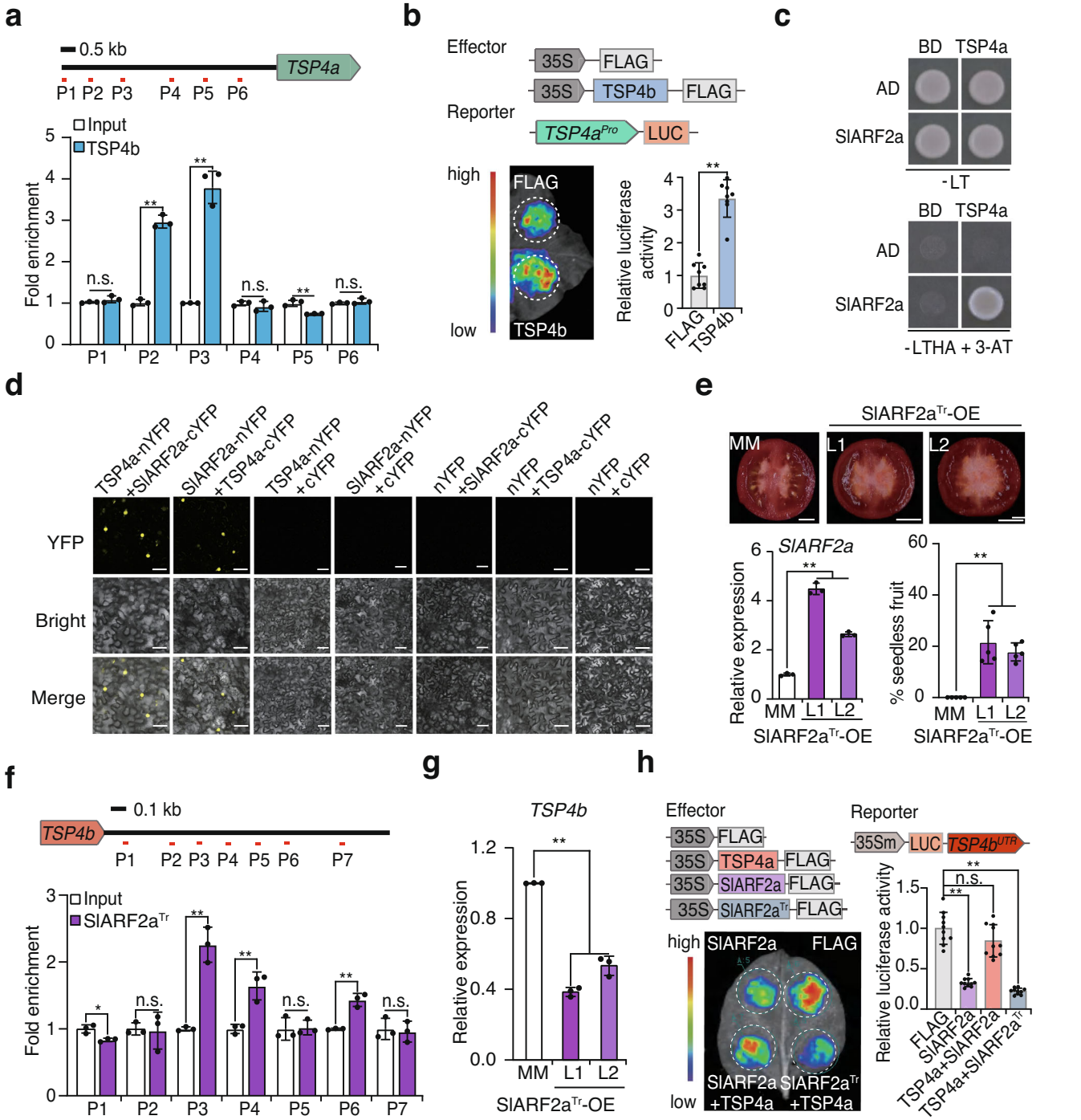

Fig. 4 | SlARF2a–TSP4a and TSP4b directly regulate the transcriptions of *TSP4b* and *TSP4a*. **a** ChIP–qPCR assay of TSP4b–YFP–HA enrichment at the *TSP4a* promoter. Schematic of promoter regions and primer-binding sites used for ChIP–qPCR (P1–6). P1 region was used as a negative control and Input was mock-IP negative control without the antibody. **b** Representative dual-luciferase reporter assay in *N. benthamiana* co-infiltrated with $35S_{pro}$:*FLAG or* $35S_{pro}$:*TSP4b–FLAG* and $TSP4a_{pro}$:*LUC-*$35S_{pro}$:*REN*. Leaves co-infiltrated with $TSP4a_{pro}$:*LUC-*$35S_{pro}$:*REN* and $35S_{pro}$:*FLAG* were used as control ($n = 8$ biologically independent replicates). **c** Yeast two-hybrid of the protein interaction between TSP4a and SlARF2a. Yeast cells were grown on -Leu/-Trp (-LT) plates and -Leu/-Trp/-Ade/-His (-LTHA) plates (containing 30 mM 3-AT) for 3 d. **d** BiFC visualization of the interaction between TSP4a and SlARF2a in the nuclei of *N. benthamiana* epidermal cells, Bars = 50 μm. Three independent experiments were conducted with similar results. **e** Fruits of Moneymaker and $35S_{pro}$:*SlARF2a*^{Tr}*–YFP–HA* over-expression lines. Scale bar = 2 cm. *SlARF2a* expression in −2 DPA ovaries and seedless fruit rate from Moneymaker and $35S_{pro}$:*SlARF2a*^{Tr}*–YFP–HA* under heat stress ($n = 5$ plants). **f** ChIP–qPCR assay of SlARF2a^{Tr}–YFP–HA enrichment at the *TSP4b* 3′ UTR. Schematics of promoter regions and primer-binding sites used for ChIP–qPCR (P1–7). P1 region was used as a negative control and Input was mock-IP negative control without the antibody. **g** *TSP4b* expression in −2 DPA ovaries isolated from Moneymaker and $35S_{pro}$:*SlARF2a*^{Tr}*–YFP–HA* plants under heat stress in the greenhouse. **h** Representative dual-luciferase reporter assay in *N. benthamiana* co-infiltrated with $35S_{pro}$:*FLAG*, $35S_{pro}$:*TSP4a–FLAG*, $35S_{pro}$:*SlARF2a–FLAG*, $35S_{pro}$:*SlARF2a*^{Tr}*–FLAG* and $35Smin_{pro}$:*LUC-*$TSP4b_{utr}$*-*$35S_{pro}$:*REN*. Leaves co-infiltrated with $35Smin_{pro}$:*LUC-*$TSP4b_{utr}$*-*$35S_{pro}$:*REN* and $35S_{pro}$:*FLAG* were used as a control ($n = 10$ biologically independent replicates). Data in (**a**, **e**–**g**) are the mean ± S.D. of $n = 3$ biologically independent replicates, qPCR and ChIP-qPCR were normalized to *UBIQ3* and *ACTIN*, respectively. Data in (**a, b, f**) were determined by two-tailed Student's *t*-test. Data in (**e**, **g**, **h**) were compared by one-way ANOVA with multiple comparisons and Tukey post-hoc test ($\alpha = 0.05$). $^{**}P < 0.01$, n.s. non-significant ($P > 0.05$). Source data are provided as a Source Data file.

https://doi.org/10.1038/s41467-025-59522-7

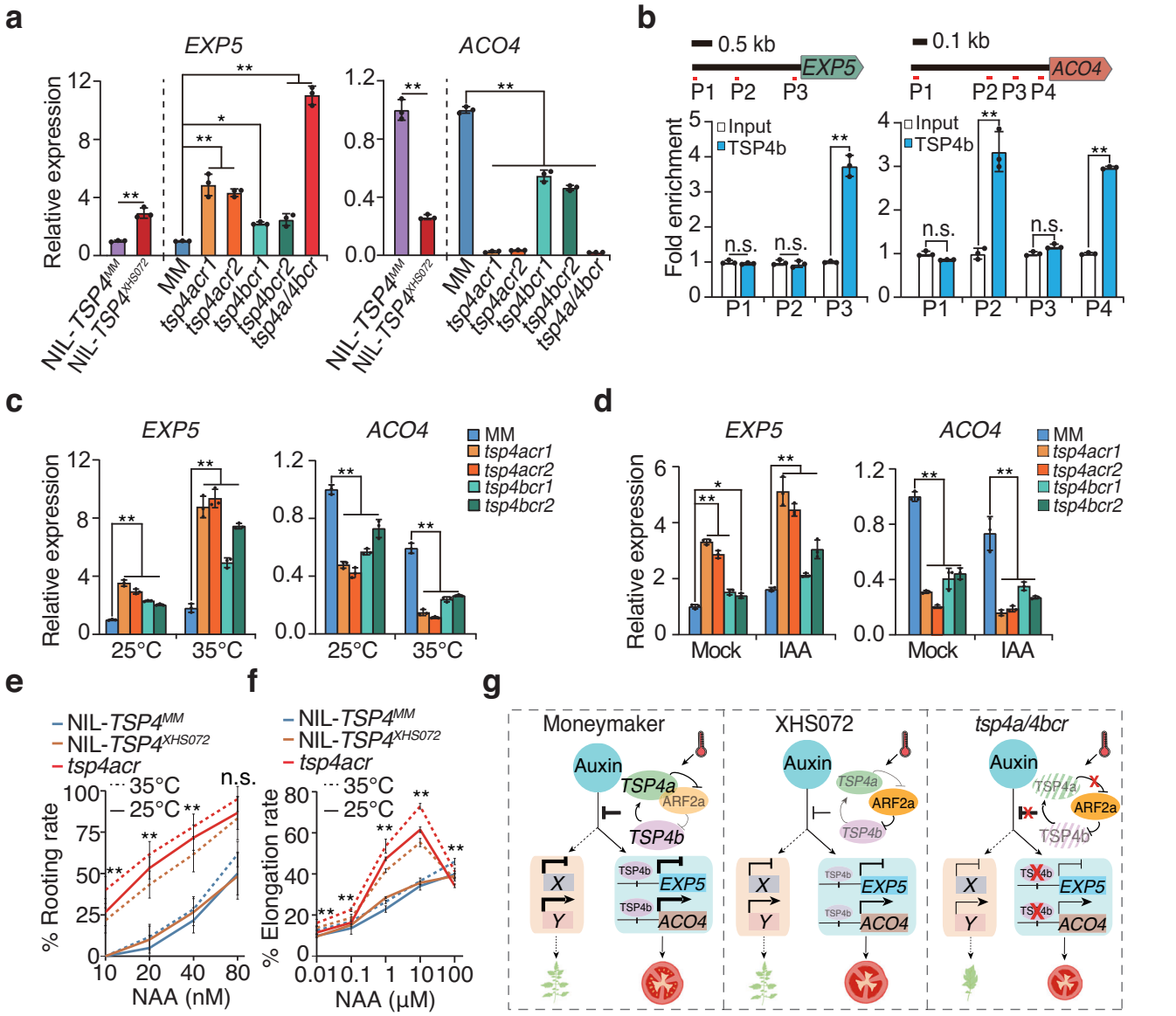

Fig. 5 | TSP4a and TSP4b co-regulate auxin-responsive genes under heat stress. **a** *EXP5* and *ACO4* expression in −2 DPA ovaries isolated from NIL-*TSP4*^{MM} and NIL-*TSP4*^{XHS072} plants and c.v. Moneymaker, *tsp4acr* single mutants, *tsp4bcr* single mutants and *tsp4a/4bcr* double mutants under heat stress. **b** ChIP–qPCR assay of TSP4b–YFP–HA enrichment at the *EXP5* and *ACO4* promoters. Schematics of promoter regions and primer-binding sites used for ChIP–qPCR (P1–3/4). P1 region within *EXP5* and *ACO4* was used as a negative control. Input was mock-IP negative control without the antibody. **c,** *EXP5* and *ACO4* in leaves of 4-leaf stage Moneymaker, *tsp4acr* and *tsp4bcr* single mutants grown at 25 °C or heat stress at 35°C for 2 h. **d** *EXP5* and *ACO4* expression in seedlings of 12-d-old Moneymaker, *tsp4acr* and *tsp4bcr* single mutants treated with the solvent (mock) or 10 μM IAA for 2 h. Auxin dose-response assays for cotyledon-explant rooting rate (**e**, $n = 10$ biologically independent replicates) and hypocotyl-segment elongation (**f**, $n = 20$ biologically independent replicates) under control (25 °C) and heat-stress (35 °C) conditions. Data in (**a**–**d**) are the mean ± S.D. of n = 3 biologically independent replicates, qPCR and ChIP-qPCR were normalized to *UBIQ3* and *ACTIN*, respectively. The effect of NIL background on relative expression and ChIP–qPCR were determined by two-tailed Student's *t*-test and the effect of genotype on relative expression and auxin dose-response were determined by one-way ANOVA with multiple comparisons and Tukey post-hoc test (α = 0.05). *$P < 0.05$, **$P < 0.01$, n.s. non-significant ($P > 0.05$). **g** Proposed model illustrating how the *TSP4a–TSP4b* positive feedback module inhibits auxin signaling and directly regulates auxin-responsive genes ('*X*' and '*Y*'), including *EXP5* and *ACO4*. TSP4b can directly activate the *TSP4a* expression, and TSP4a interacts with SlARF2a to prevent the latter from repressing *TSP4b* gene transcription. Compared with wild-type plants, disruption of *TSP4a* and *TSP4b* enhances auxin signaling, inducing parthenocarpy and causing pleiotropic phenotypes. However, weaker *TSP4a* and *TSP4b* expression from *TSP4*^{XHS072} natural alleles down-regulates auxin signaling specifically under heat stress to overcome the trade-off between fruit set and development. Source data are provided as a Source Data file.

(Assay for Transposase-Accessible Chromatin using sequencing), indicative of open chromatin[31]. Of the five *tsp4a*^{pro} alleles (Fig. 6f–j) and five *tsp4b*^{utr} alleles (Fig. 6k–o) with deletions distributed along these regulatory regions, the *tsp4a*$^{pro\text{-}4}$, *tsp4a*$^{pro\text{-}5}$ and *tsp4b*$^{utr\text{-}5}$ alleles all developed seedless fruits in the greenhouse under heat stress. This was associated with reduced *TSP4a* and *TSP4b* expression levels (Fig. 6g, h, l-m). Importantly, the parthenocarpic phenotypes were tightly associated with deletions in the second distal ATAC region in the *TSP4a* promoter and the second downstream ATAC region in the *TSP4b* 3′ UTR. Compared to Moneymaker, *tsp4a*$^{pro\text{-}4}$, *tsp4a*$^{pro\text{-}5}$ and *tsp4b*$^{utr\text{-}5}$ alleles had no obvious effects on fruit fresh weight and sugar content of red ripe fruits in the greenhouse (Fig. 6i, n, Supplementary Fig. 15c–d) and leaf morphology (Fig. 6j, o). Consistent with the increase in fruit number, the yield of these plants was also improved under heat stress compared to Moneymaker (Supplementary Fig. 15e–h). Taken together, these results further support the roles of

https://doi.org/10.1038/s41467-025-59522-7

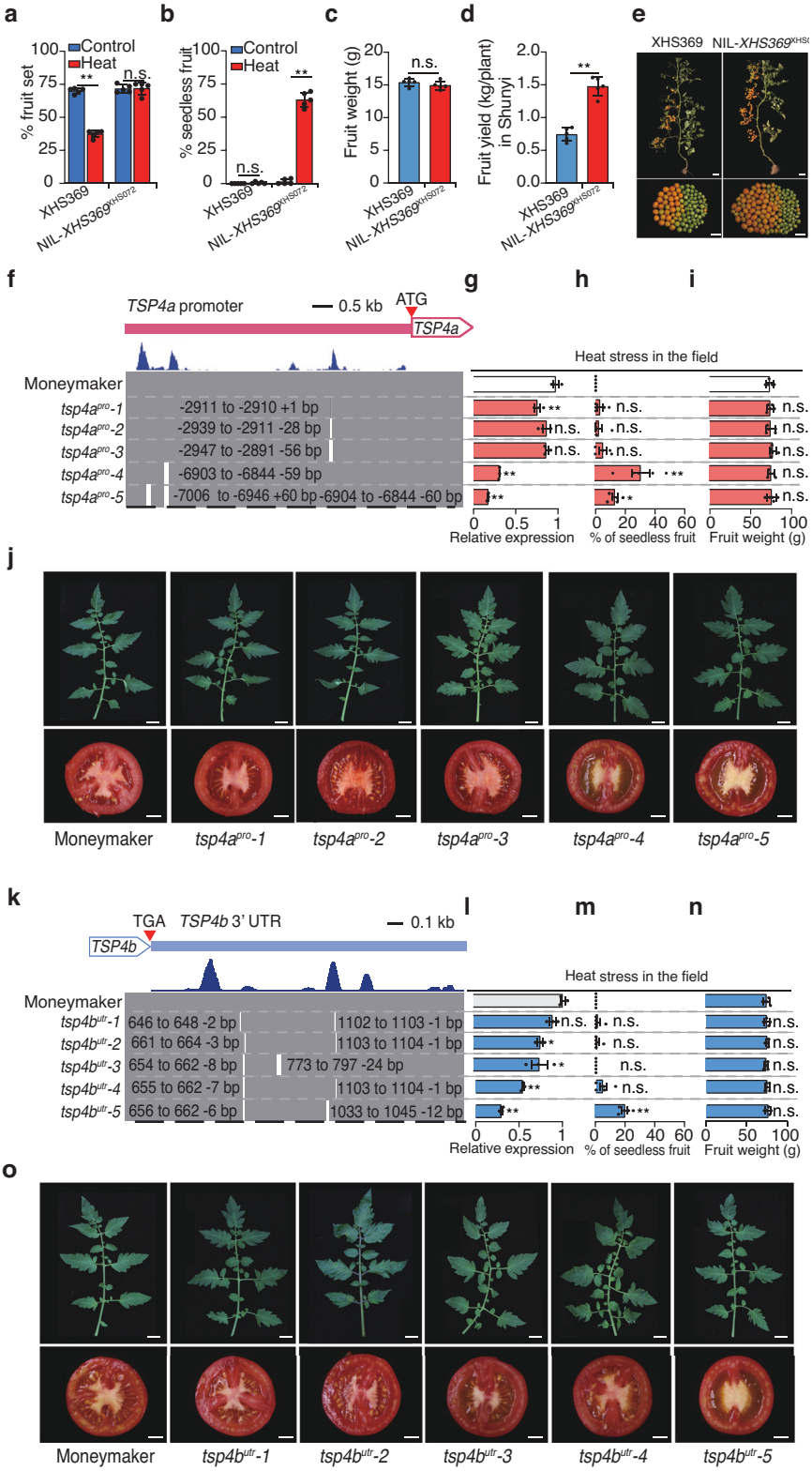

TSP4a and *TSP4b* in regulating parthenocarpic fruit set. Targeted editing of the *TSP4a* and *TSP4b* regulatory regions improves fruit-bearing ability under heat stress.

Discussion

Parthenocarpy is one of the most efficient ways to enhance yields when fruit crops face certain adverse environmental conditions and breeders have endeavored to develop parthenocarpic lines toward ensuring fruit-bearing ability[16,20,32]. Although over 10 parthenocarpic loci have been identified in tomato over the past decades[33–36], only *HB15A* and *AGL6* (underlying *pat/pat-1* and *pat-K*) have been cloned[20–22]. These two genes are involved in ovule development and also regulate seed production, therefore limiting their utility in tomato breeding in commercial settings. XHS072 is a facultative

Fig. 6 | Customization of *TSP4a* and *TSP4b* expression levels by editing regulatory regions results in conditional parthenocarpy under heat stress. Fruit-set rate (**a**) and seedless-fruit rate (**b**) for XHS369 and NIL-*XHS369*^{XHS072} plants grown under control and heat-stress conditions. Quantification of fruit weight (**c**) and fruit yield (**d**) of XHS369 and NIL-*XHS369*^{XHS072} plants grown under heat-stress conditions. **e** Plant phenotypes and fruit numbers for 120-d old XHS369 and NIL-*XHS369*^{XHS072} plants grown under heat-stress conditions, Scale bar = 10 cm. **f** Summary of indels recovered from gene editing of the *TSP4a* promoter, Blue peaks represent accessible chromatin regions. **g** *TSP4a* expression in −2 DPA ovaries isolated from wild-type Moneymaker control plants and gene-edited *tsp4a*^{pro} lines grown under heat stress. Percentage of seedless fruit (**h**) and fruit weight (**i**) for wild-type Moneymaker control plants and gene-edited *tsp4a*^{pro} lines grown under heat stress. **j** Leaves and fruits of Moneymaker and gene-edited *tsp4a*^{pro} mutant lines grown under heat-stress conditions, Scale bar = 2 cm. **k** Summary of indels recovered from gene editing the *TSP4b* 3′ UTR. Blue peaks represent accessible chromatin regions. **l** *TSP4b* expression in −2 DPA ovaries isolated from wild-type Moneymaker control plants and gene-edited *tsp4b*^{utr} lines grown under heat stress. Percentage of seedless fruit (**m**) and fruit weight (**n**) for wild-type Moneymaker control plants and the *tsp4b*^{utr} edited lines as shown in k grown under heat-stress conditions. **o** Leaves and fruits for wild-type Moneymaker and five gene-edited *tsp4b*^{utr} mutant lines grown under heat-stress conditions, Scale bar = 2 cm. Data in (**a**–**d**, **h**, **i**, **m**, **n**) are the mean ± S.D. of 5 plants. Data in (**g**, **l**) are the mean ± S.D. of 3 biologically independent replicates, and relative expression was normalized to *UBIQ3*. Data in (**a**, **b**) were determined by two-tailed Mann−Whitney−U test. Data in (**c**, **d**) were determined by two-tailed Student's *t*-test. Data in (**g**, **i**, **l**, **m**) were determined by one-way ANOVA with multiple comparisons and Tukey post-hoc test (α = 0.05). **P* < 0.05, ***P* < 0.01, n.s. non-significant (*P* > 0.05). Source data are provided as a Source Data file.

parthenocarpy accession that undergoes parthenocarpy only under heat stress. Large numbers of seeds can be produced in alleles with *TSP4*^{XHS072} genotypes grown in optimal environments because of successful fertilization. Breeders therefore, could exploit these two genes in contemporary tomato-improvement programs.

In contrast with Arabidopsis ANT, which has a prominent role in the development of ovules, flowers and shoots[26,27], the *tsp4bcr* mutants did not cause any other obvious defects except for parthenocarpy and smaller fruits. In contrast to the *entire* parthenocarpic mutant defective in *iaa9* with severe pleiotropic phenotypes such as simple leaves and small fruits[10,11,13], alleles with *TSP4*^{XHS072} eliminated the trade-off between parthenocarpy and broader aspects of fruit and plant development. Our data similarly suggest that auxin signaling in the ovaries is a consequence of transcriptional repression of *TSP4a* and *TSP4b* under heat stress. However, the different phenotypes for root generation and hypocotyl elongation between the *TSP4*^{XHS072} plants and *tsp4acr* knockout lines under distinct auxin treatments further support their differential responses to auxin.

Non-pleiotropic parthenocarpic *iaa9* transgenic lines, which express an RNAi construct from the ovary-specific promoter *Psol80/60*, hint that tissue-specific manipulation of IAA9 abundance is an effective way to improve tomato yield by inducing parthenocarpy[37]. Here, we obtained non-transgenic gene-edited alleles that induce parthenocarpic fruits only under heat stress by engineering *TSP4a* and *TSP4b cis*-regulatory elements. The clear parthenocarpic phenotypes expressed in the greenhouse by the bespoke engineered *tsp4a*$^{pro\text{-}4}$ and *tsp4b*$^{utr\text{-}5}$ lines support that changes in *TSP4a* and *TSP4b* expression levels are important for auxin-signaling responses in fruit initiation and development, and indicate that gene editing in elite germplasm is a promising approach to rapidly improve tomato genetics and safeguard fruit set in the face of climate change.

Our study reveals a regulatory mechanism in which SlARF2a unexpectedly acts as a positive regulator of auxin signaling within the TSP4a-SlARF2a-TSP4b feedback loop to govern tomato parthenocarpy. This finding challenges the established paradigm of SlARF2a as a canonical class B ARF protein, which typically suppresses auxin signaling through transcriptional repression[38–40]. However, CRISPR/Cas9-generated *slarf2a* knockout mutants in the Moneymaker background also exhibited pronounced parthenocarpic phenotypes (Supplementary Fig. 16), consistent with previous reports of parthenocarpy induction upon SlARF2a silencing[12]. The paradoxical convergence of parthenocarpic phenotypes in both loss-of-function *slarf2a* mutants and *SlARF2a*^{Tr} overexpression transgenic plants is reminiscent of the dual regulatory functions observed in SlARF8A and 8B during tomato parthenocarpy[15]. Similar to the PB1-domain-deficient ARF8A/8B overexpression lines[15], our SlARF2a^{Tr} transgenic plants likely achieve their phenotypic effects through competitive interference with endogenous auxin signaling components. These parallel findings challenge the binary classification of ARF proteins as activators or repressors. Instead, our results reveal an unexpected context-dependent functional plasticity within the ARF proteins.

In addition to auxin, ethylene also plays a role in suppressing tomato fruit set by modifying gibberellin metabolism[41]. *ACO4* encodes an ACC oxidase, which catalyzes the conversion of 1-aminocyclopropane-1-carboxylic acid (ACC) to ethylene[42]. In the *iaa9-3* mutant, low expression levels of *ACO4* result in a decrease of ethylene content in fruit[41]. Our results showed that the expression level of *ACO4* is also dramatically reduced in the *tsp4acr* and *tsp4bcr* mutants. Consistent with this, ethylene content is reduced in these mutants compared to that of wild-type Moneymaker (Supplementary Fig. 17). Thus, parthenocarpy is a complex process that involves interactions among different hormone pathways.

In conclusion, we discovered two genes conditionally conferring parthenocarpy in tomatoes under heat stress by optimizing auxin signaling during fruit initiation and development via a tightly controlled feedback loop. The practical utility of this approach was validated in our graded mutant series with varying degrees of *TSP4a* and *TSP4b* down-regulation that display durable parthenocarpy in the rigors of the greenhouse and maintain desired fruit sugar contents, demonstrating translational potential to engineer elite varieties favored by industry with high yield to cope with global climate change.

Methods

Plant materials, growth conditions

Seeds of *Solanum lycopersicum* c.v. Moneymaker was obtained from the C.M. Rick Tomato Genetics Resource Center (TGRC; https://tgrc.ucdavis.edu) at the University of California, Davis. Seeds of XHS072 were obtained from our own stocks. Seeds for all studies were sown in 32-square plug trays filled with a mixture of peat and vermiculite (3:1). Seedlings of parental lines, NILs, recombinant lines and transgenic plants were grown in a growth chamber under the following conditions: 16:8 h light:dark photoperiod, 26/20 °C (day/night) temperature with 300 µmol photons m^{-2} s^{-1} irradiance and 60–70% humidity. Thirty-day-old seedlings were transplanted to a greenhouse at the Shunyi experimental station (116°87′ E, 40°17′ N) in Beijing, China. Temperature in the greenhouse was monitored and the conditions were as follows: for the typical (i.e. control) temperature, plants were grown in a greenhouse from March to May, a daily mean temperature of 24 °C with a peak temperature of 27 °C, and for the high temperature (i.e. heat stress), the plants were grown in a greenhouse from May to August, a daily mean temperature of 32 °C with a peak temperature of 40 °C. For a greenhouse at the Nankou experimental station (116°5′ E, 40°13′ N) in Beijing, China. Temperature in the greenhouse was monitored, and the conditions were as follows: for the high temperature (i.e., heat stress), the plants were grown in a greenhouse from August to October, a daily mean temperature of 33.72 °C with a peak temperature of 40.4 °C.

Nicotiana benthamiana seeds were sown in 32-square plug trays filled with a mixture of peat and vermiculite (3:1). Seedlings were

grown in a growth chamber under the following conditions: 16:8 h light:dark photoperiod, 26/20 °C (day/night) temperature with 300 μmol photons m^{-2} s^{-1} irradiance, 60–70% humidity. Four-week-old seedlings were used for experiments.

Plants sampled for qRT–PCR analysis and auxin dose-response experiments were grown in controlled conditions in growth chambers (Ruihua, AR800) with 12-h light/12-h dark cycle at 26/22°C day/night temperatures, and high-temperature conditions of 12-h light/12-h dark cycle with 35/26 °C day/night temperatures, with 250 μmol photons m^{-2} s^{-1} irradiance.

Emasculation of flowers and phenotypic analysis

The artificial emasculation experiment was done as described previously with some modifications[13]. −2 DPA flowers on mature tomato plants (two to four weeks after the first flowering) were emasculated, and the presence of only pectin and no seeds in the red ripe fruits was considered parthenocarpy. For fruit-bearing ability and parthenocarpy quantification, more than five individual plants of each accession were phenotyped. The fruits of each plant were evaluated without artificial pollination. The percentage of seedless fruit represents the proportion of seedless fruit to the total number of fruits, with 10–40 fruits per plant typically scored. The percentage of fruit set represents the proportion of fruit to the number of flowers. Fruit weight (g) represents the average fruit fresh weight of red ripe fruit. Fruit number represents the total number of fruits per plant and fruit yield (kg) represents the average yield of all fruits fresh weight from more than five plants.

Mapping and identification of *TSP4*

Non-parthenocarpic *Solanum lycopersicum* c.v. Moneymaker and the parthenocarpic c.v. XHS072 were used as parental materials. An F_2 population was generated by crossing Moneymaker with XHS072 and 320 individual plants were used for bulk-segregant analysis (BSA)[23]. We selected 31 plants with non-parthenocarpic (seedless fruit rate 0%) and 29 plants with parthenocarpic fruit (seedless fruit rate > 30%) for BSA. Equal amounts of tissue from each plant were pooled for DNA extraction. The genomic DNA was sheared using a Diagenode Bioruptor Plus instrument to obtain ~300 bp fragments. Libraries were prepared using the NEXTflexTM Rapid DNA-Seq Kit for Illumina sequencing (NOVA-5144-08) according to the manufacturer's protocol. Genomic DNA reads were trimmed by quality using FastQC (https://www.bioinformatics.babraham.ac.uk/projects/fastqc/), and paired reads were mapped to the reference tomato genome (SL4.0) using BWA-MEM, with default parameters[43]. SNP calling was based on alignment results using the Genome Analysis Toolkit GATK 3.1.1[44].

BSA was performed with modification[45]. SNPs between two parental genomes were identified for further analysis when the base-quality value was ≥ 20 and the SNP quality value was ≥ 20. On the basis of these criteria and the number of SNPs with a read depth ≥ 5x, an SNP index was calculated for both bulk samples, expressing the proportion of reads harboring SNPs that were identical to those in the parent (Moneymaker). The ΔSNP index was obtained by subtracting the SNP index for the non-parthenocarpic bulk sample from that for the parthenocarpic bulk sample.

Near-isogenic lines (NILs) were generated by selecting heterozygous offspring at the *qTSP4* locus for selfing. After six generations, markers to identify plants homozygous for NIL-$TSP4^{MM}$ or NIL-$TSP4^{XHS072}$ were used to genotype the presence/absence of the introgressed region (860 kb) around the *TSP4* locus. On this basis, we generated six alleles with different combinations of *TSP4a* and *TSP4b* haplotypes including $TSP4a^{MM}4b^{MM}$, $TSP4a^{XHS072}4b^{MM}$, $TSP4a^{MM}4b^{XHS072}$, $TSP4a^{XHS072}4b^{MM/XHS072}$, $TSP4a^{MM/XHS072}4b^{XHS072}$ and $TSP4a^{XHS072}4b^{XHS072}$. All markers used are listed in Supplementary Data 3.

Plasmid construction and plant transformation

CRISPR–Cas9 mutagenesis was employed to target specific regions within the exons of *TSP4a*, *TSP4b*, and *SlARF2a*, as well as the promoter of *TSP4a* and the 3′ UTR of *TSP4b*. The target sites were carefully designed using the CRISPR-P tool (available at http://cbi.hzau.edu.cn/CRISPR/). Vectors were constructed according to the previously described[46]. Briefly, primers containing the designed sgRNA sequences and *Bsa*I restriction enzyme recognition sites were synthesized. These primers were used to amplify the sgRNAX_U6-26t_SlU6p_sgRNAX fragments from a pCBC_DT1T2_SlU6p vector, after which the PCR fragments were purified and cloned into pTX041 at the *Bsa*I sites[47].

For the construction of $35S_{pro}$:*TSP4a–YFP–HA* and $35S_{pro}$:*TSP4b–YFP–HA*, the coding sequences of *TSP4a* and *TSP4b* were amplified from Moneymaker cDNA template and fused to the N-terminus of *YFP–HA* using an In-fusion HD Cloning kit (Vazyme, C113)[48]. $35S_{pro}$:$SlARF2a^{Tr}$*–YFP–HA* was constructed as described previously with modifications[12,15]. The *SlARF2a* coding sequence without the PB1 domain was amplified from the Moneymaker cDNA template and fused to the N-terminus of *YFP–HA* using an In-fusion HD Cloning kit (Vazyme, C113).

All plasmids were validated by sequencing and then transformed into *Agrobacterium tumefaciens* AGL1[49]. Wild-type c.v. Moneymaker, XHS072 and NIL-$TSP4^{XHS072}$ plants were transformed in accordance with *A. tumefaciens*-mediated cotyledon-explant transformation as described previously[47] and selected on 50 mg/L kanamycin. Transgenic plants were validated by PCR and sequencing. All primers used are listed in Supplementary Data 3. *tsp4a/4bcr* double mutants in the Moneymaker background were obtained by crossing *tsp4acr1* and *tsp4bcr2* single mutants.

Auxin quantification by UPLC–MS/MS

Auxin was isolated from −2 DPA NIL-$TSP4^{MM}$ and NIL-$TSP4^{XHS072}$ ovaries grown under control and high-temperature conditions with three biological replicates. Auxin extraction and measurement were as described previously[50] with minor modifications. For each sample, 20 mg of tissue was collected into a 2 mL RNA-free centrifuge tube and ground in liquid nitrogen. Empty tubes and tubes plus samples were weighed, and then 1.8 mL chromatography-grade MeOH and 10 μg/mL D-IAA (dissolved in MeOH) were added for use as internal standards. The sample was extracted overnight at −20 °C and then centrifuged for 15 min at 13,400 *g* at 4 °C. The supernatant was then collected in a new 2 mL tube and evaporated under nitrogen gas. The residue was dissolved in 1 mL chromatography-grade ammonia solution (5%, v/v). Samples were loaded onto an Oasis MAX SPE cartridge, which was sequentially washed with 4 mL chromatography-grade ammonia solution (5%, v/v), 4 mL water then 4 mL MeOH. 4 mL of MeOH containing 10% (v/v) formic acid was used to elute samples, and eluted samples were dried. The dried residue was reconstituted in 200 μL 80% (v/v) MeOH followed by centrifugation for 30 min at 4 °C at 13,000 rpm before UPLC–MS/MS analysis.

Auxin contents were measured using Waters UPLC–MS/MS (ACQUITY UPLC I-Class-Xevo TQ-S Micro, Waters). A Waters CSH C18 column was used as the analytical column (2.1 mm × 100 mm i.d., 1.7 μm). The mobile phase consisted of 0.1% formic acid (FA) and acetonitrile (ACN) as solvent A and 0.1% FA and water as solvent B. The temperatures of the column and autosampler were 35 °C and 4 °C, respectively. Run initially with 20% A, then increase to 73% A in 1 min and increase to 78% A in the next 3 min, decrease to 20% in 1 min, keep 20% A for 2 min (total 7 min) under a flow rate of 0.2 mL/min. The content was calculated according to the internal standard method. Data analysis was performed using MassLynx V4.1 (Waters).

Quantification of ethylene production

Ethylene was isolated from Moneymaker and gene knockout mutants ovaries at −2 DPA, with three biological replicates for each group.

Ethylene extraction and measurement were as described previously with minor modifications[41]. Ethylene production rate was measured by gas chromatography–mass spectrometry (Agilent, 8890-7000E) equipped with a 30 m × 0.25 mm × 0.25 μm capillary column (HP-5ms Ultra Inert). We collected five to eight ovaries of tomatoes, weighed and enclosed them into a 2-mL glass vial, which was incubated at 25 °C for 4 h under darkness. After incubation, 10 μL of gas from the headspace of the 2 mL glass vial was injected into the gas chromatography for analysis. The temperature of injector port was 250 °C. The temperature of the column kept at 40 °C for 1 min, ramped to 100 °C at 20 °C/min, and kept at 100 °C for 1 min. The carrier gas was helium with the pressure of 12.942 psi. The injection mode was in splitless. The content was calculated according to the external standard method. Data analysis was performed using MassHunter Quantitative Analysis 12.0 (Agilent).

Fructose and glucose quantification by UPLC–-MS/MS

Fructose and glucose were isolated from more than five red ripe fruits from NILs and gene-edited lines grown under high-temperature conditions with three biological replicates. Sample pretreatment and measurement were performed as described previously[51]. Tomato samples (0.1 g) were extracted in 1.9 mL arabinose solution (1 mg/mL) by sonication (500 W, 10 min), followed by centrifugation (13,000 g, 10 min). The supernatant was double-filtered (0.22 μm PES) and mixed 1:1 with acetonitrile before analysis. Fructose and glucose contents were measured by UPLC–MS/MS (ACQUITY UPLC I-Class-Xevo TQ-S Micro, Waters). For saccharide analysis, an ACQUITY UPLC BEH Amide 1.7 μm column was used as the analytical column (2.1 x 100 mm; Waters). Sugar content was calculated according to the internal standard method. Data analysis was performed using MassLynx V4.1 (Waters).

In situ RNA hybridization

In situ RNA hybridization was performed as described with some modifications[52,53]. All procedures were conducted under stringent RNase-free conditions. The cDNA segments of *TSP4a* and *TSP4b* were amplified using primers P18 and P19 (Supplementary Data 3) and subsequently cloned into pEAZY-T3 (TransGen, CT301-01), which contains *T7* promoter sequences. In vitro transcription was then carried out using T7 RNA polymerase to generate DIG-labeled antisense and sense probes for in situ hybridization. Ovary tissues were dissected and placed in freshly prepared 4% (w/v) paraformaldehyde in phosphate-buffered saline (PBS, pH 7.2), followed by vacuum infiltration (0.06 MPa) for 30 min. The tissues were then fixed at 4 °C for 16 h. After fixation, the tissues were dehydrated through a graded ethanol series (30–100%, 90 min per step), followed by dehydration in an ethanol-HistoChoice (Sigma, H2779) series. The tissues were then embedded in Paraplast Plus (Leica, P39601095). Following embedding, 10 μm sections were cut, and hybridization with the probes was performed at 55 °C in the dark for 24-48 h. After hybridization, NBT/BCIP (*SIGMAFAST*™) was used for color development. Sections were rapidly dehydrated using a graded ethanol series (30–100%, 3 seconds per step) and mounted in 50% glycerol for microscopic analysis using an Olympus BX43 microscope.

Phylogenetic analyses

The amino-acid sequences of Arabidopsis and tomato homologs of TSP4a and TSP4b were aligned by MEGAX software. Phylogenetic trees were constructed with the aligned protein sequences using MEGAX software with the neighbor-joining method. Bootstrap values were derived from 1,000 replicates.

Haplotype analyses

SNP calling was based on alignment results using the Genome Analysis Toolkit gatk 3.1.1[44]. SNPs between Moneymaker and XHS072 genomes were identified, wherein the base quality value was ≥ 20 and the SNP quality value was ≥ 20. Haplotype analysis was performed on the 8-kb promoter region of *TSP4a* and the 2.1-Kb 3′ UTR of *TSP4b*.

Heat stress and IAA application

Heat treatment was carried out according to a previously published method[54] with modifications. To assay *TSP4a* and *TSP4b* gene expression in plants grown at 25 °C and 35 °C, seedlings were grown to the 4-leaf stage at 25 °C under 12-h light/12-h darkness and transferred to 25 °C and constant illumination for 5 d. Afterward, seedlings were transferred to 35 °C with constant illumination. Leaf samples were collected at the indicated time points for analysis.

IAA treatment was carried out according to a previously published method[55] with minor modifications. Plants were treated with either a mock treatment or 10 μM IAA and 12 d seedlings were incubated on 1/2 MS medium under 25 °C and 12-h light/12-h dark in a growth chamber. Seedlings were soaked in liquid 1/2 MS medium with or without 10 μM IAA. Samples were collected and analyzed at the indicated time points.

RNA extraction and RT–qPCR analysis

Total RNA was extracted using TRNzol Universal reagent (Tiangen, DP424). Reverse transcription was performed with TransScript® II One-Step gDNA Removal and cDNA Synthesis SuperMix (TransGen, AT311-02), using 2 μg of total RNA in 20 μL reactions under the following conditions, 42 °C for 60 min, 85 °C for 10 s. Real-time quantitative PCR (RT–qPCR) was performed with 10 μl of 2*x* Taq Pro Universal SYBR qPCR Master Mix (Vazyme, Q712-02) and 5 μl cDNA on a Bio-Rad CFX-96 Real-Time PCR instrument with the following program: 3 min at 95 °C followed by 40 cycles of 20 s at 95 °C, 30 s at 60 °C, and 20 s at 72 °C. *UBI3* (*Solyc01g056940*) was used as the reference gene for normalize relative expression[54]. All primers used for RT–qPCR are listed in Supplementary Data 3.

RNA-seq analysis

Total RNA was isolated from −2 DPA NIL-*TSP4*^{MM} and NIL-*TSP4*^{XHS072} ovaries from plants grown under normal and high-temperature conditions in a growth chamber. Three biological replicates were analyzed per line, with each replicate containing at least 15 ovaries from 5 individual plants.

Twelve RNA-seq libraries were constructed and sequenced using Illumina HiSeq2000 at Berry Genomics (http://www.berrygenomics.com/). Filtered clean reads were aligned to the tomato (*Solanum lycopersicum*) cv. Heinz 1706 genome (ITAG 4.0) using STAR version 2.5.3, and their features were counted by feature Counts v 1.5.3[56]. Principal-component analysis was performed to compare the fragments per kilobase of transcript sequence per million base pairs sequenced (FPKM) values of the expressed gene using the prcomp function in R (R Foundation, Austria). Using the R package DEGseq version 3.0.3[57], the MA-plot-based method was used to calculate *P*-values that were adjusted using the Benjamini–Hochberg procedure. Gene-expression fold change between the two genotypes was calculated as FPKM. The thresholds for identification of DEGs were: FPKM > 1 in any tissue, fold change ≥ 4 or ≤ 0.25, and Benjamini–Hochberg adjusted $P < 0.001$. GO analyses of DEGs were performed using the best match homologous genes in Arabidopsis with DAVID (The Database for Annotation, Visualization, and Integrated Discovery, https://david.ncifcrf. gov).

Subcellular localization

Leaves of 40-d-old $35S_{pro}$:*TSP4a–YFP–HA* and $35S_{pro}$:*TSP4b–YFP–HA* stable-transgenic plants were used for subcellular-localization analysis. The localization of the fluorescent fusion proteins was analyzed by confocal laser-scanning microscopy (Leica DM6CS). Nuclei were detected by 10 μg/ml 4′,6-diamidino-2-phenylindole (DAPI) staining in the dark for 30 s. YFP images were captured with laser excitation at

514 nm and an emission wavelength range from 525–570 nm, and a gain value of around 600. DAPI images were captured with laser excitation at 359 nm and an emission wavelength range from 430–480 nm, and a gain value of around 600.

Auxin dose-response experiments

Auxin dose-response experiments were conducted as described previously[10] with minor modifications. Cotyledon explants of 9-d-old seedlings were cultivated in a growth chamber on MS medium containing different NAA concentrations (0 nM, 10 nM, 20 nM, 40 nM and 80 nM) at 25 °C and 35 °C for 10 d. The percentage of rooting plants represents the proportion of the number of rooted cotyledon explants to the total number of cotyledon explants after a 10-d cultivation period.

Hypocotyl fragments from 5-d-old seedlings were isolated at about 1 cm long and immediately moved into MES/sucrose buffer (5 mM MES/KOH and 1% [w/v] sucrose, pH 6.0). After 1 h pre-incubation, hypocotyl segments were randomly distributed to fresh buffer solutions with different NAA concentrations (0.01 µM, 1 µM, 10 µM, 100 µM) with gentle agitation at 25 °C and 35 °C. Elongation of hypocotyl length was measured after 23 h of treatment. The percentage elongation rate represents the proportion of the increase in final length over the initial length after 23 h of incubation.

Prediction of transcription-factor binding sites

The transcription-factor binding sites on the promoters were predicted in the JASPAR database 2024[58]. The promoter and 3′ UTR were searched for the binding sites of transcription factors using the 'Scan' function in the database. The relative profile score threshold > 80% was identified as the candidate site.

ChIP–qPCR

Chromatin immunoprecipitation (ChIP) experiment was performed as described with minor modifications[54]. −2 DPA ovaries-tissue samples (2 g) from NIL-*TSP4*^{XHS072}/*35S*$_{pro}$:*TSP4b–YFP–HA* and MM/*35S*$_{pro}$:*SlARF2a*^{Tr}*–YFP–HA* transgenic plants were immediately frozen in liquid nitrogen and ground into a fine powder under liquid nitrogen. The powdered tissue was then subjected to cross-linkage in 1% (w/v) formaldehyde (Sigma-Aldrich, 104003) for 10 min at 4 °C, followed by the addition of 0.1 M glycine, which was infiltrated for 5 min at 4 °C. Chromatin was sheared using a Diagenode Bioruptor Plus instrument to obtain ~300-bp DNA fragments. Immunoprecipitation was performed using 5 µg anti-HA antibody (Sigma, H6908). Input as a mock immunoprecipitation (mock-IP) without the antibody was used as a negative control. DNA isolated from the ChIP was used for subsequent qPCR analysis.

For ChIP–qPCR, 10 µL 2x Taq Pro Universal SYBR qPCR Master Mix (Vazyme, Q712-02) and 5 µL DNA were used on a Bio-Rad CFX-96 Real-Time PCR instrument with the following program: 3 min at 95 °C followed by 50 cycles of 20 s at 95 °C, 30 s at 60 °C, and 20 s at 72 °C. The *ACTIN* (*Solyc03g078400*) 3′ intergenic region was used as an internal control. Input DNA was used as a negative control. All primers used for qPCR are listed in Supplementary Data 3.

Dual-luciferase reporter assay

For plasmid construction, the *TSP4a*$_{pro}$:*LUC-35S*$_{pro}$:*REN*, *EXP5*$_{pro}$:*LUC-35S*$_{pro}$:*REN* and *ACO4*$_{pro}$:*LUC-35S*$_{pro}$:*REN* backbone vectors were obtained from pPZP211[59]. The 6.8-kb *TSP4a*, 4-kb *EXP5* and *ACO4* promoter sequences were amplified using Moneymaker genomic DNA as template and integrated into *LUC-35S*$_{pro}$:*REN* using an In-fusion HD Cloning kit (Vazyme, C113). The 2.1 kb *TSP4b* 3′ UTR was amplified using Moneymaker genomic DNA as a template and constructed into the *35S*$_{minpro}$:*LUC-35S*$_{pro}$:*REN* vector to obtain the *35S*$_{minpro}$:*LUC-TSP4b*$_{utr}$*-35S*$_{pro}$ vector. The *35S*$_{pro}$:*TSP4a–FLAG*, *35S*$_{pro}$:*TSP4b–FLAG*, *35S*$_{pro}$:*SlARF2a–FLAG* and *35S*$_{pro}$:*SlARF2a*^{Tr}*–FLAG* (a truncated variant of ARF2a lacking the PB1 domain) vectors were constructed using the full-length or truncated coding sequence of *TSP4a*, *TSP4b* and *SlARF2a*, respectively. All sequences were amplified from Moneymaker cDNA as a template and cloned into the *pCAMBIA2300-p35S:FLAG* vector[48]. All plasmids were validated by Sanger sequencing and transformed into *A. tumefaciens* EHA105[49]. A single colony was cultured in LB medium with appropriate antibiotic selection until $OD_{600\ nm}$ = 1.0. *Agrobacteria* were collected by centrifugation (3214 x *g*, 10 min, 20 °C) and re-suspended in 10 mM $MgCl_2$ and 150 µM acetosyringone until the $OD_{600\ nm}$ = 1. Cells containing the effector plasmids, luciferase reporter plasmid, and P19 plasmid were mixed in a ratio of 2:1:3 (v/v/v) and infiltrated into *N. benthamiana* leaves using a syringe. The leaves were harvested and ground in liquid nitrogen 36 h after infiltration.

The 1 mM luciferin substrate was spread evenly on the underside of the leaves and allowed to dry for 5 min in the dark. Subsequently, luciferase activity signals were detected with the plant in vivo imaging system (LB985 NightSHADE, Germany). Firefly luciferase (LUC) and Renilla (REN) activities were measured using a dual-luciferase reporter assay system (Promega; E1910) on a Promega GLOMAX 20/20 luminometer. REN activities were used as an internal control. Primers used to generate the constructs are listed in Supplementary Data 3.

Yeast two-hybrid

Yeast two-hybrid assays were conducted following the Yeastmaker™ Yeast Transformation System 2 user manual (Clontech, PT1172-1). To explore interactions between TSP4a and SlARF2a, the full-length coding sequence of *TSP4a* was cloned into bait vector pGBKT7, while the full-length and truncated coding sequences of *SlARF2a* were cloned into prey vectors pGADT7. The bait and prey plasmids were then cotransformed into the Y2H Gold yeast strain, following the protocol outlined in the Clontech yeast handbook instructions. The resulting transformants were grown on selective plates lacking leucine and tryptophan for 3 d at 30 °C. The interactions were evaluated by growth assays on medium lacking leucine, tryptophan, histidine, and adenine but supplemented with 30 mM 3-Amino-1,2,4-triazole (3-AT), and the growth was monitored for 3 to 5 days.

Bimolecular fluorescence complementation (BiFC) assays

The full-length coding sequences of *TSP4a*, along with the full-length coding sequence of *SlARF2a*, or truncated coding sequence of *SlARF2a*^{Tr} and *SlARF2a*^{PB1,} were amplified and subsequently inserted into the pEarleyGate 201-YN or pEarleyGate 202-YC vectors (using *Pac*I and *Spe*I restriction enzymes)[60], utilizing the In-Fusion HD Cloning Kit (Vazyme, C113). These vectors were subsequently transformed into the *A. tumefaciens* EHA105, and *TSP4a* fusion proteins were mixed with intact and truncated *SlARF2a* fusion proteins in an equal volume of culture and injected into the leaves of 4-week-old *N. benthamiana* plants. Two days after infiltration, YFP fluorescence was observed using a Leica DM6 CS confocal laser-scanning microscope. Images were captured with a laser excitation wavelength of 514 nm, and collection bandwidth was set between 525–570 nm, with intensity values around 10 and gain value of around 600. All primers used to generate the constructs are listed in Supplementary Data 3.

Statistical analyses

Two-tailed Student's *t*-test and two-tailed Mann–Whitney–U test were used to determine statistical significance using GraphPad Prism 8. For comparisons of multiple groups, the data were analyzed by one-way and two-way analysis of variance (ANOVA) followed by Tukey's multiple comparison test using GraphPad Prism 8.

Reporting summary

Further information on research design is available in the Nature Portfolio Reporting Summary linked to this article.

Data availability

The sequencing data generated in this study have been deposited in the NCBI Sequence Read Archive (SRA) database under accession SRR2391865 (Moneymaker DNA-seq), PRJNA1248730 (XHS072 DNA-seq), PRJNA1247138 (BSA-seq) and PRJNA1068180 (RNA-seq). Source data are provided with this paper.

References

1. Zhao, C. et al. Temperature increase reduces global yields of major crops in four independent estimates. *Proc. Natl Acad. Sci. USA* **114**, 9326–9331 (2017).
2. Picken, A. J. F. A review of pollination and fruit set in the tomato (Lycopersicon esculentum Mill. *J. Hortic. Sci.* **59**, 1–13 (1984).
3. Peet, M. M., Willits, D. H. & Gardner, R. Response of ovule development and post-pollen production processes in male-sterile tomatoes to chronic, sub-acute high temperature stress. *J. Exp. Bot.* **48**, 101–111 (1997).
4. Sato, S., Peet, M. M. & Thomas, J. F. Physiological factors limit fruit set of tomato (*Lycopersicon esculentum* Mill.) under chronic, mild heat stress. *Plant Cell Environ.* **23**, 719–726 (2000).
5. ReportLinker. Tomatoes Global Market Report 2023. *Globe-Newswire News Room*. https://www.globenewswire.com/en/newsrelease/2023/06/21/2692386/0/en/Tomatoes-Global-Market-Report-2023.html (2023).
6. Ayankojo, I. T. & Morgan, K. T. Increasing air temperatures and its effects on growth and productivity of tomato in South Florida. *Plants* **9**, 1245 (2020).
7. Sharif, R., Su, L., Chen, X. & Qi, X. Hormonal interactions underlying parthenocarpic fruit formation in horticultural crops. *Hortic. Res.* **9**, uhab024 (2022).
8. Gustafson, F. G. Inducement of fruit development by growth-promoting chemicals. *Proc. Natl Acad. Sci. USA* **22**, 628–36 (1936).
9. Pandolfini, T., Molesini, B. & Spena, A. Molecular dissection of the role of auxin in fruit initiation. *Trends Plant Sci.* **12**, 327–329 (2007).
10. Wang, H. et al. The tomato Aux/IAA transcription factor *IAA9* is involved in fruit development and leaf morphogenesis. *Plant Cell* **17**, 2676–92 (2005).
11. Zhang, J. et al. A single-base deletion mutation in *SlIAA9* gene causes tomato (*Solanum lycopersicum*) *entire* mutant. *J. Plant Res.* **120**, 671–8 (2007).
12. Breitel, D. A. et al. AUXIN RESPONSE FACTOR 2 intersects hormonal signals in the regulation of tomato fruit ripening. *PLoS Genet* **12**, e1005903 (2016).
13. Hu, J., Israeli, A., Ori, N. & Sun, T. P. The interaction between DELLA and ARF/IAA mediates crosstalk between Gibberellin and Auxin signaling to control fruit initiation in tomato. *Plant Cell* **30**, 1710–1728 (2018).
14. Liu, S. et al. Tomato AUXIN RESPONSE FACTOR 5 regulates fruit set and development via the mediation of auxin and gibberellin signaling. *Sci. Rep.* **8**, 2971 (2018).
15. Hu, J., Li, X. & Sun, T. P. Four class A AUXIN RESPONSE FACTORs promote tomato fruit growth despite suppressing fruit set. *Nat. Plants* **9**, 706–719 (2023).
16. Israeli, A. et al. Modulating auxin response stabilizes tomato fruit set. *Plant Physiol.* **192**, 2336–2355 (2023).
17. Molesini, B., Pandolfini, T., Rotino, G. L., Dani, V. & Spena, A. *Aucsia* gene silencing causes parthenocarpic fruit development in tomato. *Plant Physiol.* **149**, 534–48 (2009).
18. Ren, Z. et al. The auxin receptor homologue in *Solanum lycopersicum* stimulates tomato fruit set and leaf morphogenesis. *J. Exp. Bot.* **62**, 2815–26 (2011).
19. Hawthorn, L. R. Seedlessness in tomatoes. *Science* **85**, 199 (1937).
20. Clepet, C. et al. The *miR166-SlHB15A* regulatory module controls ovule development and parthenocarpic fruit set under adverse temperatures in tomato. *Mol. Plant* **14**, 1185–1198 (2021).
21. Klap, C. et al. Tomato facultative parthenocarpy results from *SlAGAMOUS-LIKE 6* loss of function. *Plant Biotechnol. J.* **15**, 634–647 (2017).
22. Takisawa, R. et al. The parthenocarpic gene *Pat-k* is generated by a natural mutation of *SlAGL6* affecting fruit development in tomato (*Solanum lycopersicum* L.). *BMC Plant Biol.* **18**, 72 (2018).
23. Takagi, H. et al. QTL-seq: rapid mapping of quantitative trait loci in rice by whole genome resequencing of DNA from two bulked populations. *Plant J.* **74**, 174–83 (2013).
24. de Jong, M., Mariani, C. & Vriezen, W. H. The role of auxin and gibberellin in tomato fruit set. *J. Exp. Bot.* **60**, 1523–32 (2009).
25. Ueta, R. et al. Rapid breeding of parthenocarpic tomato plants using CRISPR/Cas9. *Sci. Rep.* **7**, 507 (2017).
26. Klucher, K. M., Chow, H., Reiser, L. & Fischer, R. L. The *AINTEGUMENTA* gene of Arabidopsis required for ovule and female gametophyte development is related to the floral homeotic gene *APETALA2*. *Plant Cell* **8**, 137–53 (1996).
27. Mizukami, Y. & Fischer, R. L. Plant organ size control: *AINTEGUMENTA* regulates growth and cell numbers during organogenesis. *Proc. Natl Acad. Sci. USA* **97**, 942–7 (2000).
28. Guilfoyle, T. J. Aux/IAA proteins and auxin signal transduction. *Trends Plant Sci.* **3**, 205–207 (1998).
29. Nole-Wilson, S. & Krizek, B. A. DNA binding properties of the Arabidopsis floral development protein AINTEGUMENTA. *Nucleic Acids Res.* **28**, 4076–82 (2000).
30. Mockaitis, K. & Estelle, M. Auxin receptors and plant development: a new signaling paradigm. *Annu. Rev. Cell Dev. Biol.* **24**, 55–80 (2008).
31. Hendelman, A. et al. Conserved pleiotropy of an ancient plant homeobox gene uncovered by cis-regulatory dissection. *Cell* **184**, 1724–1739.e16 (2021).
32. Gorguet, B., van Heusden, A. W. & Lindhout, P. Parthenocarpic Fruit Development in tomato. *Plant Biol.* **7**, 131–139 (2005).
33. Philouze, J. & Milesi, M. Natural parthenocarpy in tomato .4. Study of parthenocarpy with polygenic determinism of line 75/59. *Agronomie* **9**, 63–75 (1989).
34. Beraldi, D., Picarella, M. E., Soressi, G. P. & Mazzucato, A. Fine mapping of the parthenocarpic fruit (*pat*) mutation in tomato. *Theor. Appl. Genet.* **108**, 209–16 (2004).
35. Gorguet, B. et al. Mapping and characterization of novel parthenocarpy QTLs in tomato. *Theor. Appl. Genet.* **116**, 755–67 (2008).
36. Nunome, T. Map-based cloning of tomato parthenocarpic *pat-2* gene. *Regul. Plant Growth Dev.* **51**, 37–40 (2016).
37. Kim, J. S., Ezura, K., Lee, J., Ariizumi, T. & Ezura, H. Genetic engineering of parthenocarpic tomato plants using transient *SlIAA9* knockdown by novel tissue-specific promoters. *Sci. Rep.* **9**, 18871 (2019).
38. Ulmasov, T., Hagen, G. & Guilfoyle, T. J. Activation and repression of transcription by auxin-response factors. *Proc. Natl Acad. Sci. USA* **96**, 5844–9 (1999).
39. Okushima, Y., Mitina, I., Quach, H. L. & Theologis, A. AUXIN RESPONSE FACTOR 2 (ARF2): a pleiotropic developmental regulator. *Plant J.* **43**, 29–46 (2005).
40. Choi, H. S., Seo, M. & Cho, H. T. Two TPL-binding Motifs of ARF2 are involved in repression of Auxin responses. *Front Plant Sci.* **9**, 372 (2018).
41. Shinozaki, Y. et al. Ethylene suppresses tomato (*Solanum lycopersicum*) fruit set through modification of gibberellin metabolism. *Plant J.* **83**, 237–51 (2015).
42. Kende, H. Ethylene biosynthesis. *Annu. Rev. Plant Biol.* **44**, 283–307 (1993).
43. Li, H. & Durbin, R. Fast and accurate short read alignment with Burrows-Wheeler transform. *Bioinformatics* **25**, 1754–60 (2009).
44. Zhang, S. et al. Detection of major loci associated with the variation of 18 important agronomic traits between *Solanum pimpinellifolium* and cultivated tomatoes. *Plant J.* **95**, 312–323 (2018).

45. Lin, T. et al. Genomic analyses provide insights into the history of tomato breeding. *Nat. Genet* **46**, 1220–6 (2014).
46. Wang, X. et al. Antagonistic regulation of target genes by the SISTER OF TM3-JOINTLESS2 complex in tomato inflorescence branching. *Plant Cell* **35**, 2062–2078 (2023).
47. Deng, L. et al. Efficient generation of pink-fruited tomatoes using CRISPR/Cas9 system. *J. Genet. Genom.* **45**, 51–54 (2018).
48. Hu, B. et al. LEAF TIP NECROSIS1 plays a pivotal role in the regulation of multiple phosphate starvation responses in rice. *Plant Physiol.* **156**, 1101–15 (2011).
49. Hwang, H. H., Yu, M. & Lai, E. M. Agrobacterium-mediated plant transformation: biology and applications. *Arabidopsis Book* **15**, e0186 (2017).
50. Fu, J., Chu, J., Sun, X., Wang, J. & Yan, C. Simple, rapid, and simultaneous assay of multiple carboxyl containing phytohormones in wounded tomatoes by UPLC-MS/MS using single SPE purification and isotope dilution. *Anal. Sci.* **28**, 1081–7 (2012).
51. Li, R. et al. *FIS1* encodes a GA2-oxidase that regulates fruit firmness in tomato. *Nat. Commun.* **11**, 5844 (2020).
52. Liu, X. et al. *AGAMOUS* terminates floral stem cell maintenance in Arabidopsis by directly repressing *WUSCHEL* through recruitment of Polycomb Group proteins. *Plant Cell* **23**, 3654–70 (2011).
53. Wang, X. T. et al. SISTER OF TM3 activates *FRUITFULL1* to regulate inflorescence branching in tomato. *Hort. Res.* **8**, 251 (2021).
54. Sun, S. et al. Genetic control of thermomorphogenesis in tomato inflorescences. *Nat. Commun.* **15**, 1472 (2024).
55. Audran-Delalande, C. et al. Genome-wide identification, functional analysis and expression profiling of the *Aux/IAA* gene family in Tomato. *Plant Cell Physiol.* **53**, 659–672 (2012).
56. Zhang, S. et al. Spatiotemporal transcriptome provides insights into early fruit development of tomato (*Solanum lycopersicum*). *Sci. Rep.* **6**, 23173 (2016).
57. Wang, L., Feng, Z., Wang, X., Wang, X. & Zhang, X. DEGseq: an R package for identifying differentially expressed genes from RNA-seq data. *Bioinformatics* **26**, 136–8 (2010).
58. Rauluseviciute, I. et al. JASPAR 2024: 20th anniversary of the open-access database of transcription factor binding profiles. *Nucleic Acids Res.* **52**, D174–d182 (2024).
59. Hajdukiewicz, P., Svab, Z. & Maliga, P. The small, versatile pPZP family of Agrobacterium binary vectors for plant transformation. *Plant Mol. Biol.* **25**, 989–94 (1994).
60. Lu, Q. et al. Arabidopsis homolog of the yeast TREX-2 mRNA export complex: components and anchoring nucleoporin. *Plant J.* **61**, 259–70 (2010).

Acknowledgements

This work was supported by the National Key Research and Development Program of China (2022YFF1003002 to X. Cui) and the National Natural Science Foundation of China Grant (32430097 to X. Cui). We are grateful to Prof. Hong Yu (Chinese Academy of Sciences), Prof. Guosheng Xiong (Nanjing Agricultural University), Prof. Chengcai Chu (South China Agricultural University), and A. Prof. Jianchang Gao (Chinese Academy of Agricultural Sciences) for their input on the manuscript.

Author contributions

X.C. conceived the project and designed the research. X.L. carried out most of the experiments; J.W., Q.S., S.S., Y.C., G.Z., and R.L. performed some of the experiments and helped score phenotypes; S.S. helped to analyzed data and revised figures; H.W. and E.v.d.K. revised the manuscript. X.L. and X.C. wrote the manuscript.

Competing interests

The authors declare no competing interests.

Additional information

Supplementary information The online version contains supplementary material available at https://doi.org/10.1038/s41467-025-59522-7.

Correspondence and requests for materials should be addressed to Xia Cui.

Peer review information Nature Communications thanks Concha Gómez-Mena and the other, anonymous, reviewer(s) for their contribution to the peer review of this work. A peer review file is available.

Reprints and permissions information is available at http://www.nature.com/reprints

Publisher's note Springer Nature remains neutral with regard to jurisdictional claims in published maps and institutional affiliations.

Open Access This article is licensed under a Creative Commons Attribution-NonCommercial-NoDerivatives 4.0 International License, which permits any non-commercial use, sharing, distribution and reproduction in any medium or format, as long as you give appropriate credit to the original author(s) and the source, provide a link to the Creative Commons licence, and indicate if you modified the licensed material. You do not have permission under this licence to share adapted material derived from this article or parts of it. The images or other third party material in this article are included in the article's Creative Commons licence, unless indicated otherwise in a credit line to the material. If material is not included in the article's Creative Commons licence and your intended use is not permitted by statutory regulation or exceeds the permitted use, you will need to obtain permission directly from the copyright holder. To view a copy of this licence, visit http://creativecommons.org/licenses/by-nc-nd/4.0/.

© The Author(s) 2025